LA-UR-05-3321 **June 2005**

Approved for public release;
distribution is unlimited.

Title

A Preliminary Probabilistic Wildfire Risk Model for Los Alamos National Laboratory

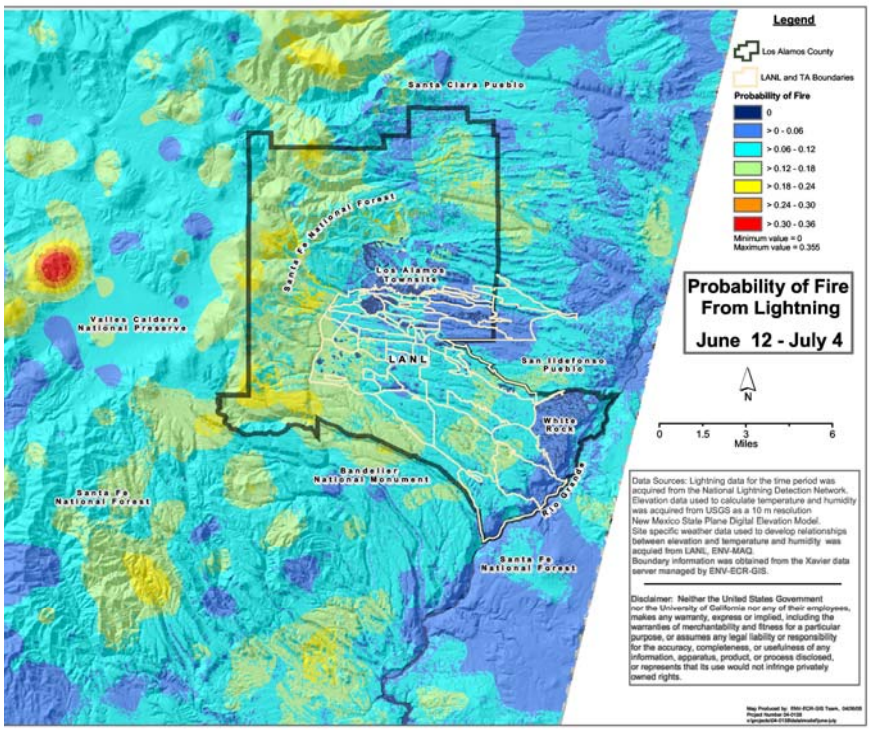

Prepared by

Randy G. Balice, Scot D. Johnson, Kathryn D. Bennett,
Todd L. Graves, Sunil Donald, Patrick D. Broxton, Wai Fung Chiu

Los Alamos
NATIONAL LABORATORY
EST. 1943

The World's Greatest Science Protecting America

Edited by Hector Hinojosa, Group IM-1

Composition by Teresa Hiteman, Group ENV-ECO

*An Affirmative Action/Equal Opportunity Employe*r

A Preliminary Probabilistic Wildfire Risk Model for Los Alamos National Laboratory

LA-UR-05-3321

Randy G. Balice, Scot D. Johnson, Kathryn D. Bennett, Todd L. Graves,
Sunil Donald, Patrick D. Broxton, Wai Fung Chiu

June 13, 2005

Abstract

Los Alamos National Laboratory is located in the eastern Jemez Mountains, New Mexico, a region that is characterized by high frequencies of wildfires. Wildfires have the potential to threaten the Laboratory by interrupting operations and by destroying life and property. However, the risks presented by wildfire are difficult to quantify. The objective of this project was to develop a preliminary, spatial-temporal modeling system that will express wildfire risks in terms of probabilities. This will facilitate the comparison and prioritization of risks for the Los Alamos region and provide a basis for management decision-making. We accomplished this objective by developing probability models and spatial algorithms of lightning-caused fires, using data representing lightning, weather, fuels, and other parameters related to wildfire hazards. The final output of the model was in the form of a probability value for each pixel in a regional land cover map. This risk value was calculated as the joint probability of 1) the occurrence of a suitable lightning flash, 2) the suitability of the ambient fuel moisture conditions for a lightning flash to result in an ignition, and 3) the potential for a lightning flash to be accompanied by the absence of ignition-extinguishing rainfall. The final risk value may be interpreted as the potential for a lightning ignition to occur and to smolder in the ground fuels for at least two days. To facilitate the calculation of risk, we defined the wildfire season as beginning on March 1 and ending on September 30. Then, we defined six segments, or subseasons, of this time period that have relatively stable weather conditions and are also distinctively different from the other subseasons. Then we created probability models for each subseason. The results of these analyses indicate that the wildfire risk from lightning strikes before April 10 is very low. The risks are higher from June 12 to July 4. The risks were low to intermediate during the other subseasons. The highest risk levels during any subseason were approximately 0.355, and these levels occurred in the mountainous areas of the Valles Caldera National Preserve. A composite risk over the entire wildfire season was also calculated and mapped. The highest composite risk was 0.49, and values in this range tended to occur in the higher elevations in the Sierra de Los Valles. With regard to the Los Alamos National Laboratory and its immediate surroundings, the greatest risks were observed in the western and southwestern portions of the Laboratory and in the adjacent mountainous areas.

Introduction

Problem statement

Los Alamos National Laboratory (LANL) and its neighboring communities of Los Alamos and White Rock are located in a fire-prone region (Touchan et al. 1996). In addition, accumulations of fuels in the forests and woodlands of the region during the past century have increased the potential for high-intensity fires to occur (Balice et al. 1999, 2000). The ability of these wildfires to cause damage, lost productivity, and even loss of life has been demonstrated by recent wildfires, such as the Dome Fire and the Cerro Grande Fire (Balice 1996, Site-wide Issues Program Office 2000). The costs of the impacts from these disturbances, along with subsequent rehabilitation activities, can be extraordinary (U.S. Department of Energy 2000). The continuation of uninterrupted operations at LANL depends in part on the maintenance of fire hazards at acceptably low levels. Much progress toward this goal has been achieved in the past seven years. However, this progress is difficult to quantify, and it is not currently possible to objectively document the distributions of residual wildfire risks.

Previous work in the Los Alamos region

Previous attempts to characterize the risks to LANL from wildfire have been based on field documentations of fire hazard levels, the development of descriptive scenarios based on field data and expert opinion, and statistical analyses of weather data. The Site-wide Environmental Impact Statement for Continued Operation of the Los Alamos National Laboratory (U.S. Department of Energy 1999) determined the frequency of a large fire encroaching on LANL by estimating the joint probability of ignition in forested vegetation to the west of LANL, high to extreme fire danger, failure to promptly extinguish the fire, and a three-day period of weather that would promote severe wildfires. The analysis concluded “that a major fire moving up to the edge of LANL is not only credible but likely, probably on the order of 0.1 per year” (U.S. Department of Energy 1999:G-105).

Field monitoring to assess wildfire hazards from fuel levels has also been employed. For instance, inventories and surveys of fuels and vegetational structures in forests and woodlands during 1997 were used to characterize the fire hazards in the Los Alamos region (Balice et al. 1999). These data were also combined with knowledge of weather patterns during the Los Alamos fire season to develop a “most credible wildfire scenario” (Balice et al. 1999:19) that would threaten LANL or burn on LANL property. This scenario was found to be consistent with three fires, Water Canyon, La Mesa, and Dome, which burned in the Los Alamos region and threatened LANL between 1950 and 1996. This scenario was also consistent with the progression of the Cerro Grande Fire, which burned in May of 2000 (U.S. Department of Energy 2000).

Lightning is a major cause of wildfires and data of the frequency, intensity, and spatial distributions of lightning can be used to develop probabilistic risk models. This was demonstrated in an analysis to address human safety at the Dual-axis Radiographic Hydrodynamic Test (DARHT) facility at LANL (Bott and Eisenhawer 2004). They used Monte

Carlo simulation to estimate the expected number of human fatalities for a typical experiment at the DARHT facility.

Objectives of the current study

The current project adds to these previous results by quantitatively addressing risks from wildfire and mapping these risks across the Los Alamos region. This approach facilitates the comparisons of risks at different points within the region and prioritizing treatments for reducing risks at strategic locations. We accomplished this objective by developing probability models and spatial algorithms of lightning-caused fires, using data representing lightning, weather, fuels, and other parameters related to wildfire hazards. The estimated probabilities of wildfire risk were displayed on a map to facilitate comparison, prioritization, and management decision-making.

Methods

General approach

For the purposes of this project, we adapted a general model developed by Anderson (2002). This quantitative model assumes the probability of a lightning-caused fire is the product of independent probabilities of four key steps leading to the onset of the fire. The basic form of the model with the modifications that we incorporated is given below:

$$p_{fire}(t) = p_{LCC}\, p_{ign}\, p_{sur}\, p_{arr},$$

where

$p_{fire}(t)$ = the probability that at least one lightning-caused fire will be ignited and smolder during a specified time period *t*,

p_{LCC} = the probability of at least one lightning flash with a long-continuing current (LCC),

p_{ign} = the probability of ignition assuming a lightning flash with an LCC,

p_{sur} = the probability of survival for the ignition to continue in a smolder state for at least two days, and

p_{arr} = the probability of arrival for the smoldering fire to a flaming state.

To develop a model for the Los Alamos region, we modified the first three terms of the probability model, p_{LCC}, p_{ign}, and $p_{sur}(t)$, to accommodate the data that are available for the region and to maintain consistency with conditions that influence the potential for wildfire in the Southwest. We did not explicitly incorporate p_{arr} into the model. For the purposes of this project, the first three terms of the model represent respectively 1) the probability of the occurrence of a suitable lightning flash, 2) the probability that the ambient fuel moisture conditions are suitable for a lightning flash to result in an ignition, and 3) the probability that any rainstorm that accompanies the lightning flash is not sufficient to extinguish the ignition. Since we are not treating p_{arr}, we implicitly make the conservative assumption that this term and any additional transition states that follow, such as the probability that fire spreads or that a building burns, are equal to one.

Data available for this project

Lightning data for the development of p_{LCC} were obtained by the National Lightning Detection Network (NLDN). These data had been compiled by the Tucson Operations Office, Vaisala, Inc. (Cummins et al. 1998). A cloud-to-ground lightning event is recorded by the NLDN as an initial stroke, which is then typically followed by one or more return strokes (Bott and Eisenhawer 2004). Lightning data obtained from Vaisala, Inc., can be limited to data that pertain to the initial stroke, or may also include data for each of the associated strokes that follow. These are known, respectively, as flash data and stroke data. The median location accuracy of both flash and stroke data is 500 meters or less (Cummins et al. 1998). The average lightning flash and stroke detection efficiency are 95 percent and 78 percent, respectively (Kehoe and Krider 2004).

The Nuclear Design and Risk Analysis Group at LANL obtained NLDN flash data for the years 1994 to 1999 and for 2001 (Bott and Eisenhawer 2004). This dataset includes all recorded flashes within 100 kilometers (60 miles) of the DARHT facility and their location (latitude and longitude), the polarity (positive or negative), and the peak current (kiloamps).

Knowledge of fuels, fire hazards, and weather conditions throughout the Los Alamos region were required to develop statements of the probability of ignition p_{ign} and the probability of survival $p_{sur}(t)$. The Ecology Group has been monitoring and characterizing fuels and fire hazards in forests and woodlands of the Los Alamos region since 1977 (Balice et al. 1999, 2000). The Ecology Group also developed land cover classifications used in this project (Koch et al. 1997, Balice et al. 1997, Balice 1998). The land cover classification was modified and used to classify a Landsat image from June 4, 2001 (McKown et al. 2003). The image was smoothed to 0.25 hectare minimum polygon size. The entire extent of the land cover map was used as the study area for this project (Figure 1). The land cover types used to classify the map are listed in Table 1.

Weather data were made available through a system of six weather-monitoring towers in the Los Alamos region (Baars et al. 1998, Rishel et al. 2003). These towers for monitoring weather conditions are maintained by the Meteorology and Air Quality Group. They collect a variety of data types including temperature, precipitation, windspeed, and lightning occurrences. Most of these towers are identified by the LANL Technical Area (TA) in which they are located (Table 2). Five of these towers occupy locations near the perimeter of LANL or adjacent to Los Alamos and White Rock (Figure 2). The sixth tower is located near the summit of Pajarito Mountain.

Definition of wildfire subseasons

In this project, we defined the wildfire season for the Los Alamos region to begin on March 1 and to continue to September 30, during which wildfires can occur at any time. However, the weather conditions favoring or disfavoring wildfire are not constant throughout the wildfire season. Therefore, we used 1) historical lightning activity, 2) windspeeds, and 3) rainfall, summarized on a daily basis, to define wildfire subseasons within the time period from March 1 to September 30. A fourth source of information, the average length of daylight for each candidate period, was also used to define and characterize the wildfire subseasons. The goal of this subseason definition process was to develop subseasons that are relatively stable and distinct from other subseasons.

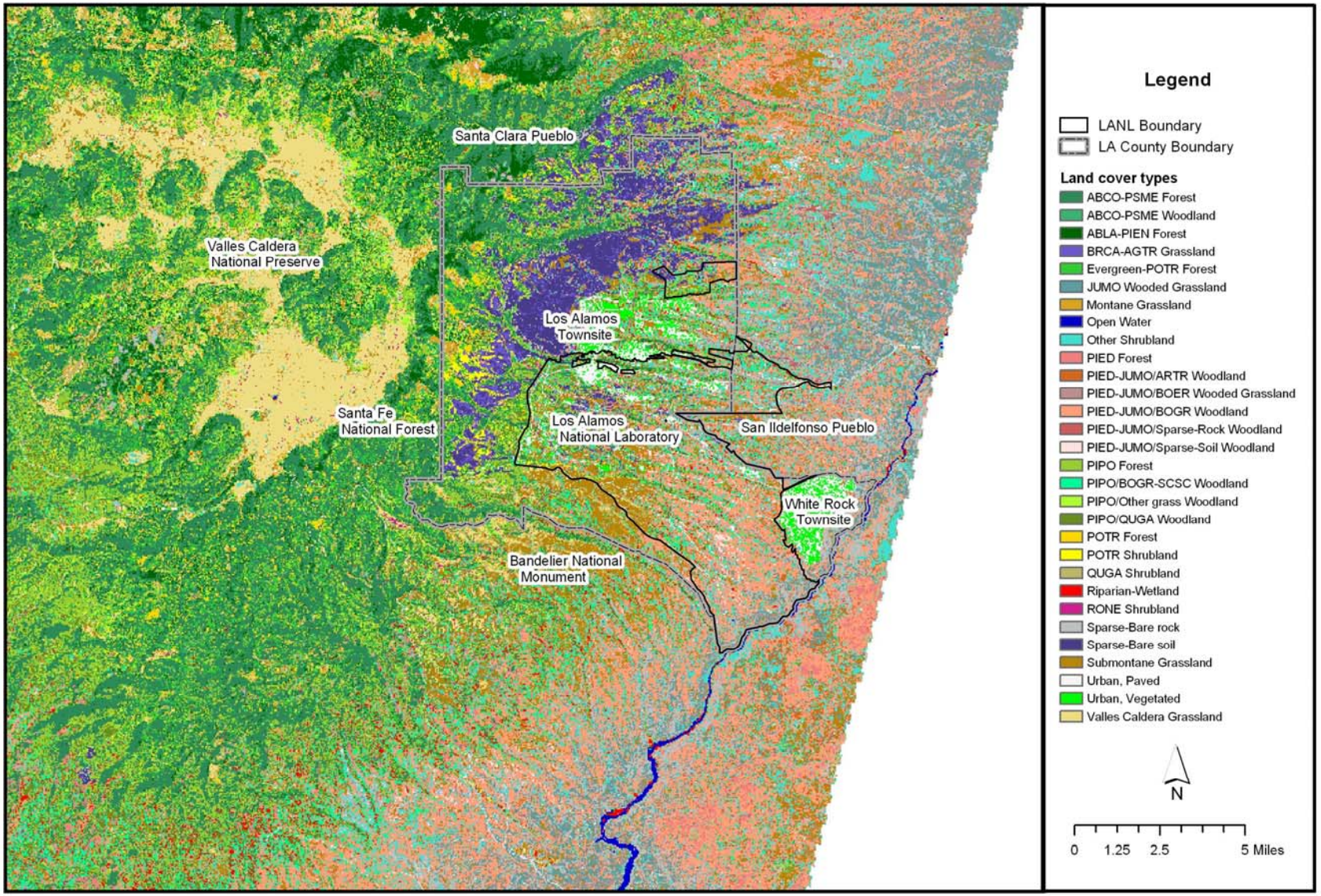

Figure 1. Land cover map used for assignment of wildfire hazards (McKown et al. 2003). (NOTE: See Table 1 footnote for key.)

Table 1. Cover classes used to classify the land cover map used in this study (McKown et al. 2003).

Class number	Cover class*	Hectares	Acres	Square miles	Square kilometers	Percent
29	RONE Shrubland	113.06	279.39	0.44	1.13	0.06
16	PIED-JUMO/Sparse-Rock Woodland	267.75	661.62	1.03	2.68	0.15
14	PIED-JUMO/Sparse-Soil Woodland	383.20	946.92	1.48	3.83	0.21
25	POTR Shrubland	445.59	1101.07	1.72	4.46	0.24
7	Open water	446.36	1102.97	1.72	4.46	0.25
9	Riparian-Wetland	943.67	2331.85	3.64	9.44	0.52
32	Urban, Paved	976.88	2413.92	3.77	9.77	0.54
31	Urban, Vegetated	1247.65	3083.00	4.82	12.48	0.69
18	PIED-JUMO/ARTR Woodland	1354.98	3348.21	5.23	13.55	0.74
26	POTR Forest	1467.37	3625.93	5.67	14.67	0.81
2	Montane Grassland	1816.80	4489.40	7.01	18.17	1.00
20	BRCA-AGTR Grassland	2030.08	5016.43	7.84	20.30	1.11
19	PIED-JUMO/BOER Wooded Grassland	2343.03	5789.74	9.05	23.43	1.29
3	ABCO-PSME Woodland	2785.95	6884.21	10.76	27.86	1.53
30	PIED Forest	3784.85	9352.53	14.61	37.85	2.08
27	PIPO/Other grass Woodland	4048.34	10003.65	15.63	40.48	2.22
6	Sparse-Bare soil	4466.50	11036.94	17.25	44.67	2.45
13	QUGA Shrubland	4563.47	11276.55	17.62	45.63	2.51
5	Evergreen-POTR Forest	5813.44	14365.29	22.45	58.13	3.19
10	Sparse-Bare Rock	6433.55	15897.61	24.84	64.34	3.53
24	ABLA-PIEN Forest	6522.16	16116.56	25.18	65.22	3.58
17	Other Shrubland	7091.70	17523.94	27.38	70.92	3.89
12	PIPO/BOGR-SCSC Woodland	7606.81	18796.78	29.37	76.07	4.18
28	JUMO Wooded Grassland	8432.53	20837.19	32.56	84.33	4.63
23	PIPO/QUGA Woodland	8472.20	20935.22	32.71	84.72	4.65
15	Submontane Grassland	8485.56	20968.22	32.76	84.86	4.66
1	Valles Caldera Grassland	11409.91	28194.43	44.05	114.10	6.27
21	PIPO Forest	14475.24	35769.00	55.89	144.75	7.95
11	PIED-JUMO/BOGR Woodland	28080.23	69387.58	108.42	280.80	15.42
4	ABCO-PSME Forest	35804.05	88473.50	138.24	358.04	19.66
Sums		**182112.91**	**450009.64**	**703.14**	**1821.13**	**100.00**

* RONE = *Robinia neomexicana*; PIED = *Pinus edulis*; JUMO = *Juniperus monosperma*; POTR = *Populus tremuloides*; ARTR = *Artemisia tridentata*; BRCA = *Bromus carinatus*; AGTR = *Agropyron trachycaulum*; BOER = *Bouteloua eriopodoa*; ABCO = *Abies concolor*; PSME = *Pseudotsuga menziesii*; PIPO = *Pinus ponderosa*; QUGA = *Quercus gambelii*; ABLA = *Abies lasiocarpa*; PIEN = *Picea engelmannii*; BOGR = *Bouteloua gracilis*; SCSC = *Schizachyrium scoparium.*

Table 2. LANL weather tower location information (Meteorology and Air Quality Group 2001).

Tower	Longitude	Latitude	Elevation (m)	Elevation (ft)
TA-54	106° 13' 22.1"	35° 49' 32.8"	1996.3	6548
TA-41	106° 17' 45.1"	35° 52' 35.0"	2107.9	6914
TA-53	106° 15' 13.4"	35° 52' 12.4"	2131.1	6990
TA-49	106° 17' 55.5"	35° 48' 47.8"	2147.9	7045
TA-6	106° 19' 8.4"	35° 51' 41.1"	2263.4	7424
Pajarito Mountain	106° 23' 43.5"	35° 53' 11.2"	3158.5	10,360

The specific fire weather variables that were used to define the individual fire weather subseasons are listed below:

1) Average daily windspeed (meters/second) and average maximum daily wind gusts (meters/second). The data were obtained at the TA-6 weather tower from 1990 to 2004 (Figure 3).

2) Average daily windspeed (meters/second) and average maximum daily wind gusts (meters/second). The data were obtained at the TA-54 weather tower from 1992 to 2004 (Figure 4).

3) Total daily number of cloud-to-cloud and cloud-to-ground lightning strokes ($\log_{10}$) detected within a radius of approximately 30 miles. The data were obtained at the TA-6 weather tower from 1998 to 2004 (Figure 5).

4) Fraction of days with measurable precipitation during a 60-year precipitation record. One fraction exists for each calendar day. A second fraction of days with measurable precipitation plus traces of precipitation (a trace is not measurable). The second fraction is always larger than the first, which includes only measured precipitation. The data were obtained at the TA-6 weather tower and two nearby weather monitoring stations that preceded the initiation of data collection at TA-6. The precipitation data span the period from 1945 to 2004 (Figure 6). To enhance the interpretive qualities of Figure 6, 0.2 was added to each value of fraction of days with daily measurable plus trace precipitation.

5) The number of daylight hours for each day of the year was obtained from the Collaboratory Project (Northwestern University 2005). From these data, the average number of daylight hours was calculated for each candidate subseason.

The resulting wildfire subseasons were defined as a result of the analyses of the data in Figure 3 to Figure 6. The beginning and end of each wildfire subseason is indicated in each of the figures by vertical, dashed lines and with consecutive subseason numbers. General descriptions of each wildfire subseason follow and are also summarized in Table 3.

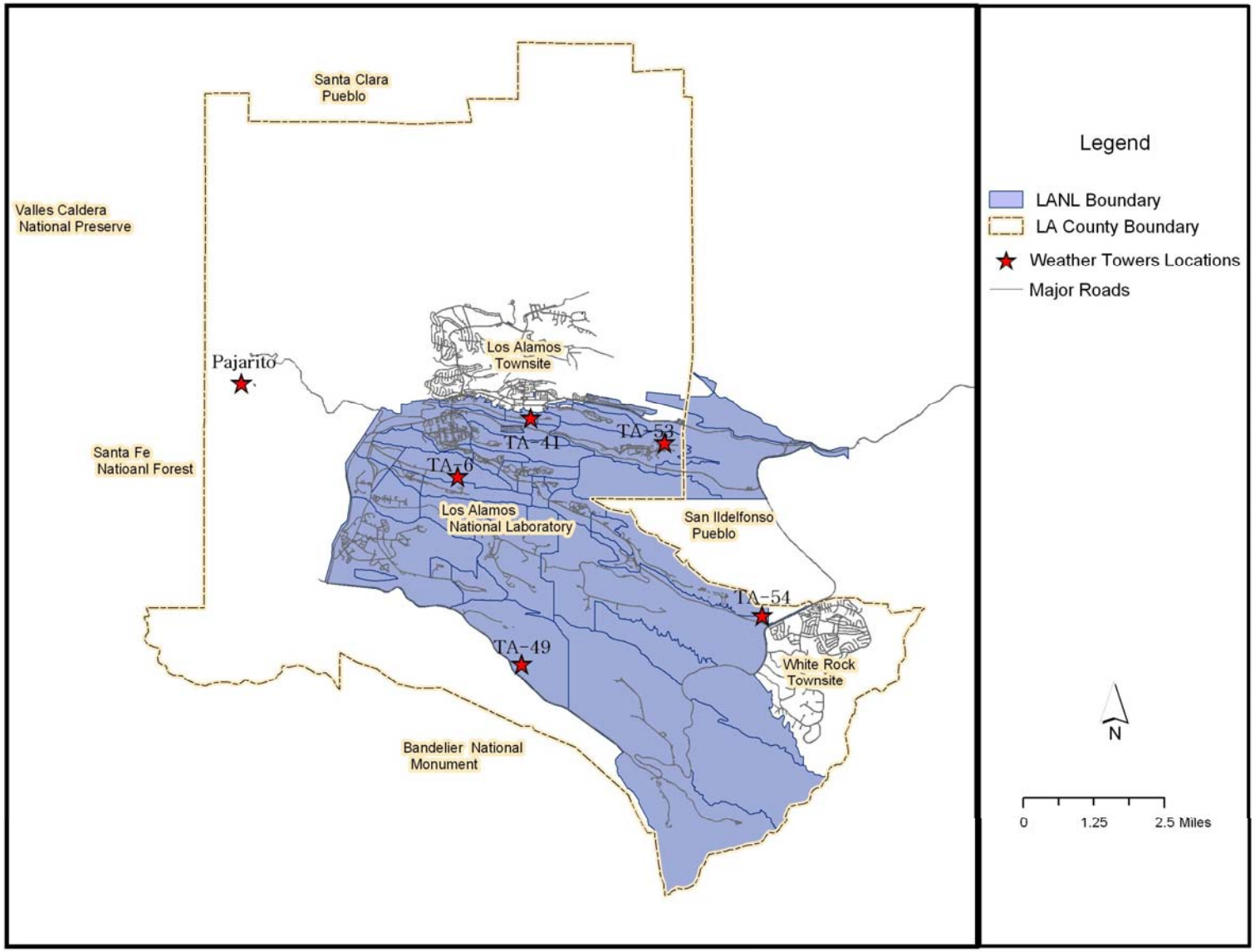

Figure 2. Locations of weather monitoring towers in the Los Alamos region (Rishel et al. 2003).

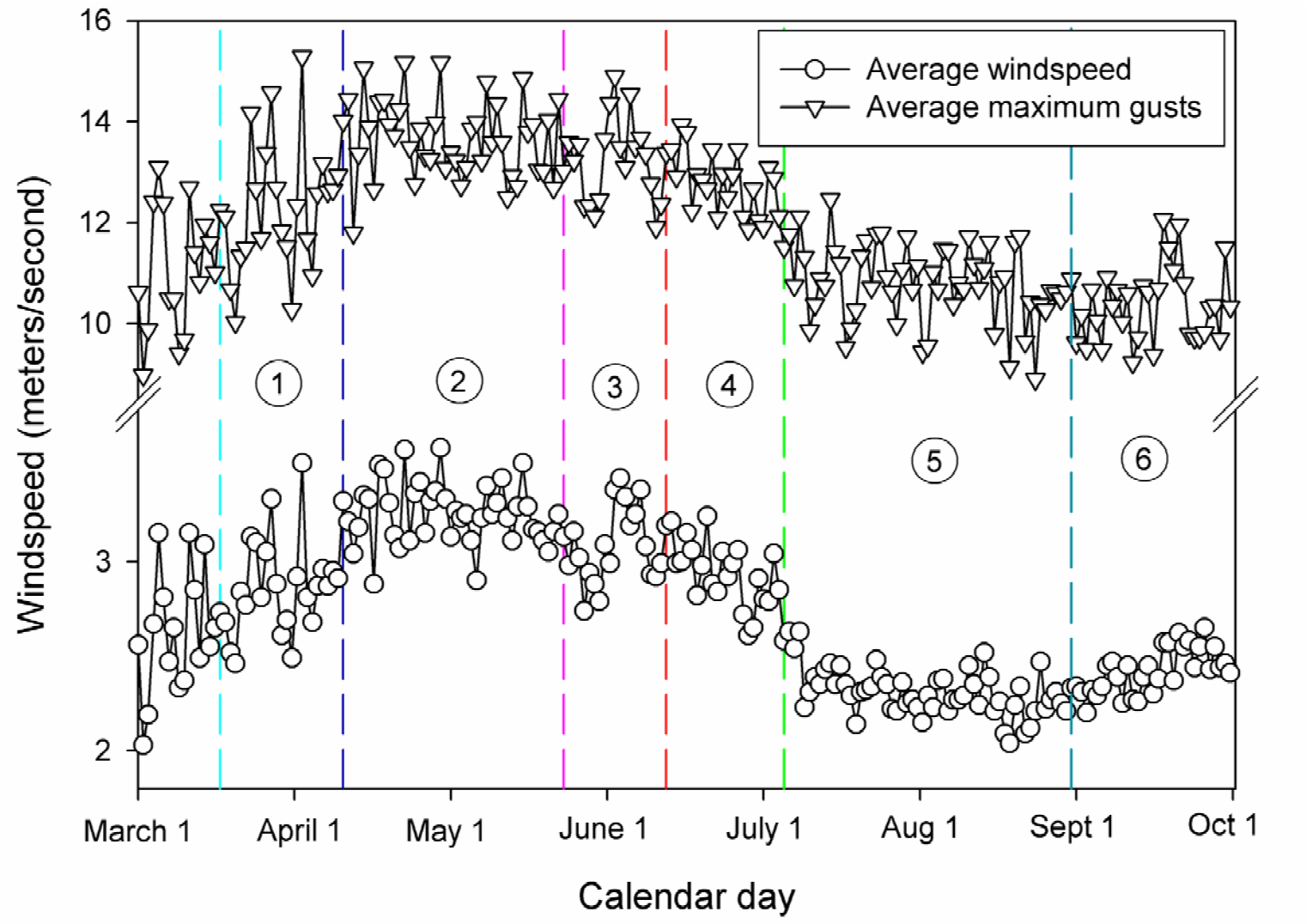

Figure 3. Average windspeed and average speed of maximum daily wind gusts at TA-6 from 1990 to 2004. The colored vertical lines and circled numbers define the six wildfire subseasons, beginning March 17 and ending September 30.

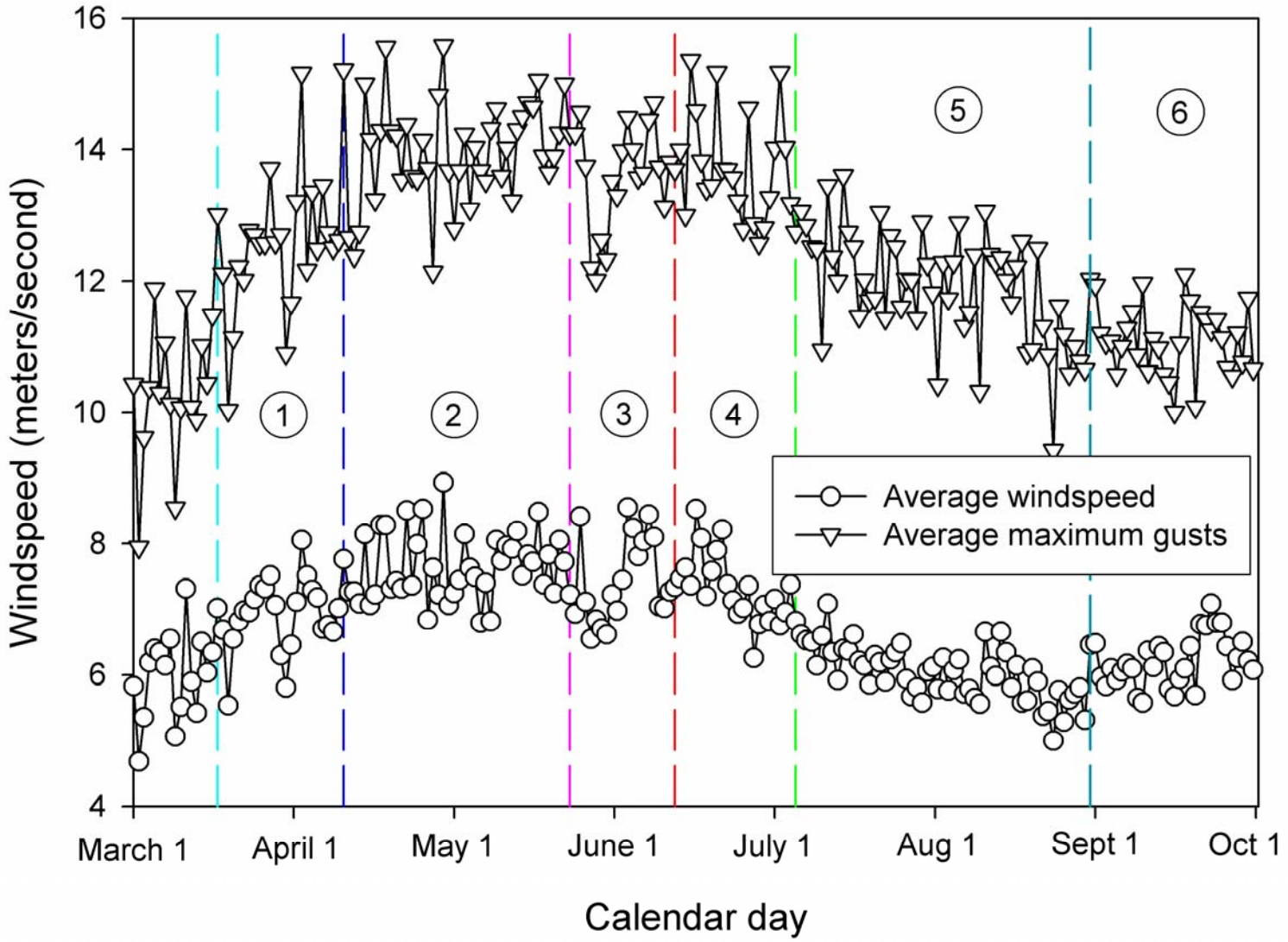

Figure 4. Average windspeed and average speed of maximum daily wind gusts at TA-54 from 1992 to 2004. The colored vertical lines and circled numbers define the six wildfire subseasons, beginning March 17 and ending September 30.

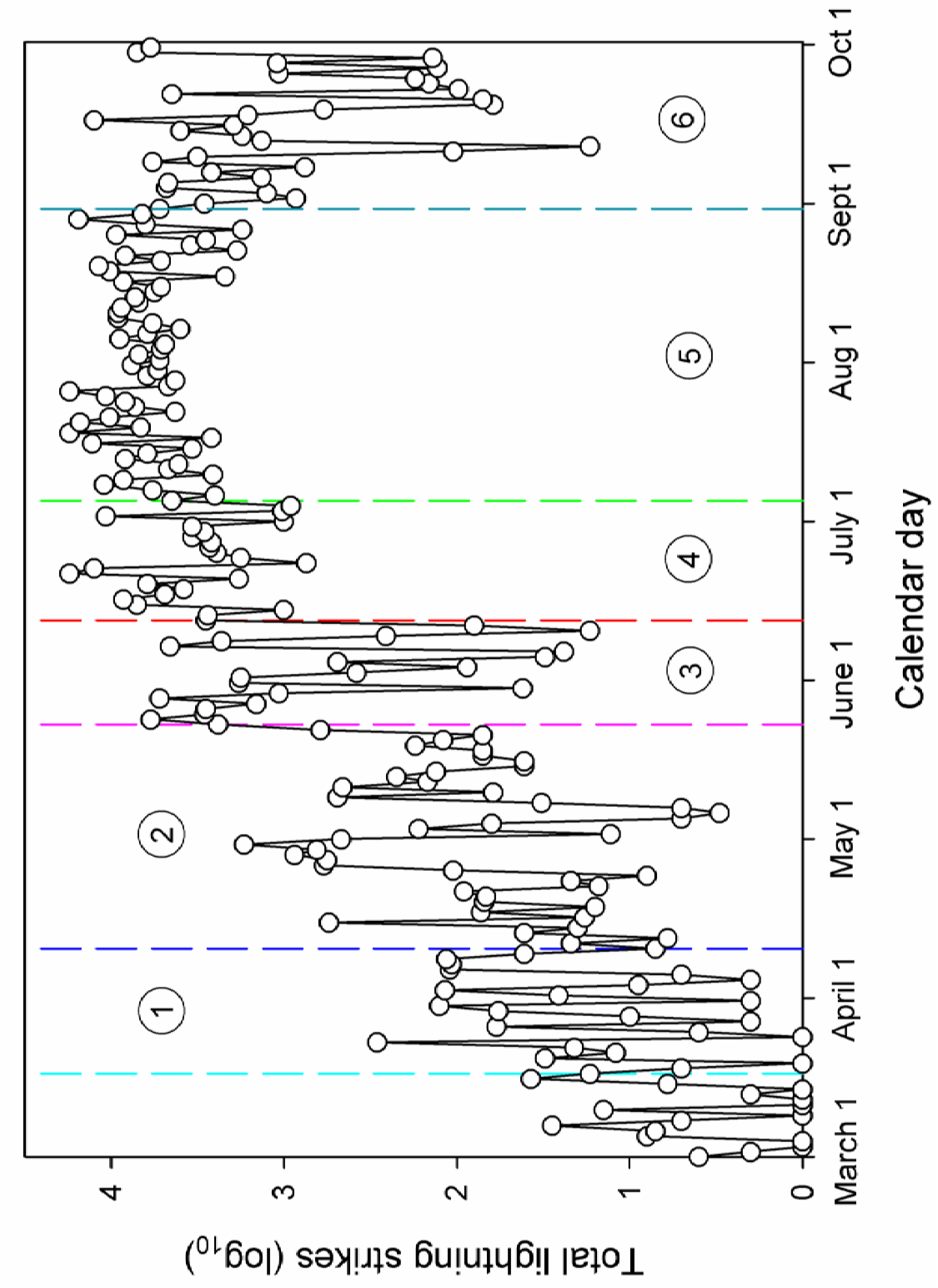

Figure 5. Total lightning strikes (log_{10}) at TA-6 from 1998 to 2004. The colored vertical lines and the circled numbers define the six wildfire subseasons, beginning March 17 and ending September 30.

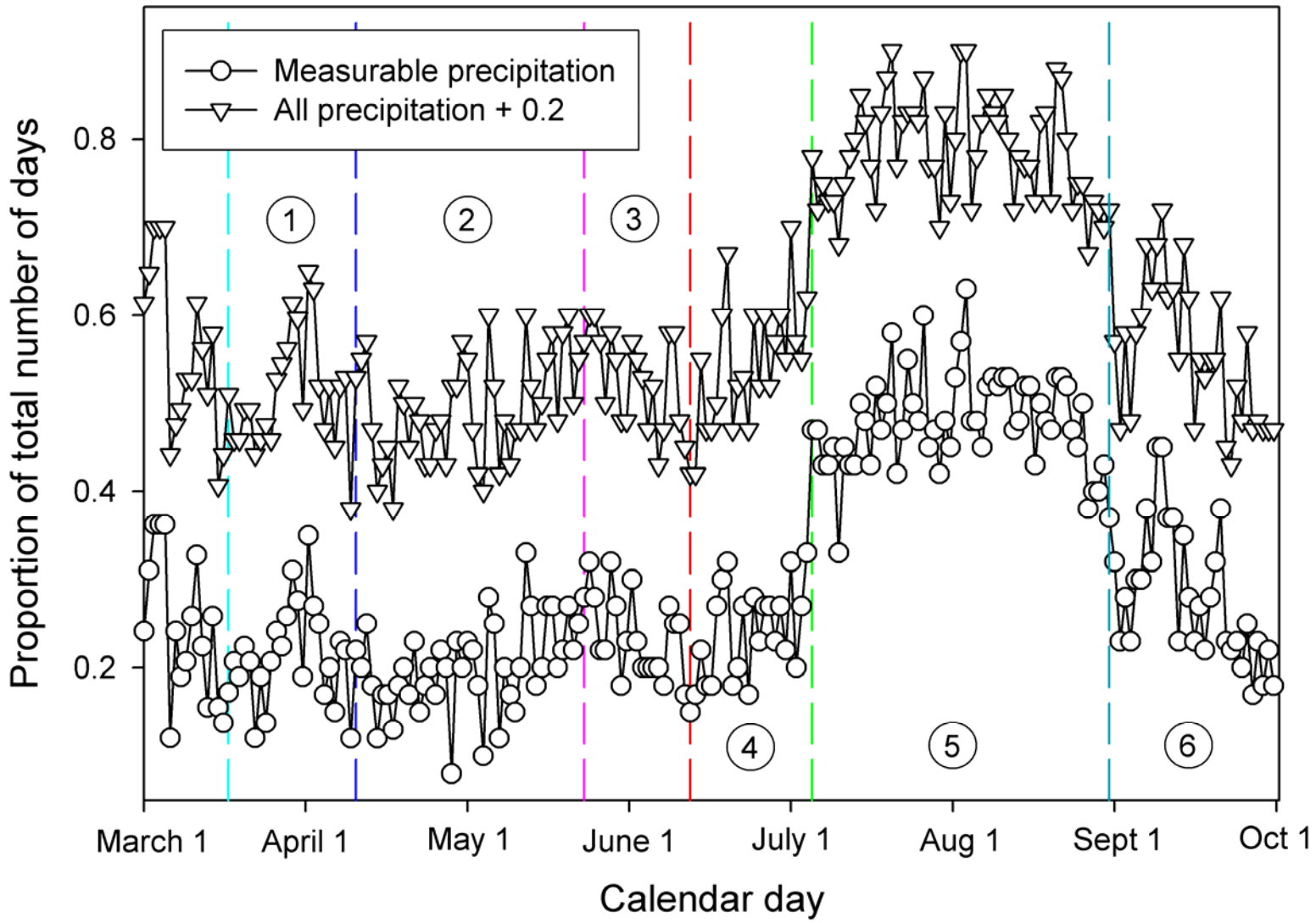

Figure 6. Daily precipitation levels in the Los Alamos region from 1945 to 2004. Measurable precipitation excludes days with trace amounts. All precipitation includes trace amounts with 0.2 added for separation between the two plots. The colored vertical lines and the circled numbers define the six wildfire subseasons, beginning March 17 and ending September 30.

Table 3. Definitions and general descriptions of wildfire subseasons.

Subseason	Undefined	1	2	3	4	5	6
Wildfire Threat	Very low	Low	Moderate	High	Very High	Moderate	Low
Time Period	March 1 – March 16	March 17 – April 9	April 10 – May 22	May 23 – June 11	June 12 – July 4	July 5 – August 30	August 31 – September 30
Number of Days	16	24	43	20	23	57	31
Windspeed	Low	Increasing	High	High	Moderate	Low	Low
Lightning	Low	Increasing	Increasing	High but variable	High	Very High	Decreasing and variable
Precipitation	Low	Low	Low	Low	Moderate	High	Moderate to Low
Average Daylight Period	11 hrs 43 min	12 hrs 27 min	13 hrs 35 min	14 hrs 21 min	14 hrs 29 min	13 hrs 48 min	12 hrs 22 min

Subseason not defined; relatively little threat from wildfire. March 1 to March 16 (Number of days = 16). Windspeeds are low, lightning activity is low, and precipitation is low. This time period will not be analyzed further in this project. The average daylight period is 11 hours 43 minutes.

Subseason 1 (S1); low wildfire threat. March 17 to April 9 (Number of days = 24). Windspeeds and lightning activity are both increasing. Precipitation levels are low. The average daylight period is 12 hours 27 minutes.

Subseason 2 (S2); moderate wildfire threat. April 10 to May 22 (Number of days = 43). Windspeeds are high. Lightning activity continues to increase. Precipitation levels remain low. The average daylight period is 13 hours 35 minutes.

Subseason 3 (S3); high wildfire threat. May 23 to June 11 (Number of days = 20). Windspeeds are high. Lightning activity is high but variable. Precipitation levels remain low. The average daylight period is 14 hours 21 minutes.

Subseason 4 (S4); very high wildfire threat. June 12 to July 4 (Number of days = 23). Windspeeds are decreasing from high to moderate. Lightning activity is high. Precipitation levels are increasing from low to moderate. The average daylight period is 14 hours 29 minutes.

Subseason 5 (S5); moderate wildfire threat. July 5 to August 30 (Number of days = 57). Windspeeds are decreasing from moderate to low. Lightning activity is very high. Precipitation levels are high. The average daylight period is 13 hours 48 minutes.

Subseason 6 (S6); low wildfire threat. August 31 to September 30 (Number of days = 31). Windspeeds are low. Lightning activity is decreasing and variable. Precipitation levels are moderate to low. The average daylight period is 12 hours 22 minutes.

Lightning and its relation to wildfire ignitions

Lightning is a complex event. Attempts to incorporate lightning into probability models of wildfire risk must account for this complexity and isolate the characteristics of lightning that most influence the potential for lightning to ignite wildfires. The most basic characterization of this complexity is in terms of flash events and stroke events. "A *flash* is a lightning discharge in its totality; the average duration of a flash is 0.5 sec. A *stroke* is partial discharge consisting of a downward-moving leader streamer of low luminous intensity followed by an upward-moving return streamer of high luminous intensity. A flash may consist of a single stroke or a series of strokes in the same or adjacent channels" (Kitagawa et al. 1962:638).

In addition to the complexity imparted by the number of strokes per flash, individual lightning events vary with respect to their polarity and the amount of energy that is imparted to the earth. A lightning flash where the luminosity decays abruptly after each stroke and involves only nominal amounts of energy overall "is called a *discrete flash*" (Kitagawa et al. 1962:639). However, the intensity of a lightning flash can be amplified to high levels if one or more strokes are associated with a continuing current or an "M component" (Uman 1987). Continuing current usually occurs in lightning flashes that consist of multiple strokes. The continuing current flows in the channel after individual strokes. The flow of continuing current may continue for more than a tenth of a second.

The time interval of each continuing current in a lightning stroke has received much attention. A continuing current episode of more than 40 milliseconds has been called a long continuing current (LCC) or a long continuing stroke (Kitagawa et al. 1962, Brook et al. 1962). In contrast, lightning with continuing current components between 10 milliseconds and 40 milliseconds are called short continuing currents or short continuing strokes (Shindo and Uman 1989). A continuing current event ranging from 1 to 10 milliseconds in duration is called a possible continuing current or a questionable continuing current.

Lightning events that include strokes with "long-continuing current… transfer about twice the charge that flashes without long-continuing current do. From a practical point of view, the effect of continuing current on objects struck by lightning is to cause potentially serious heating damage" (Uman 1987:169). LCC is of special interest because it is apparently responsible for the bulk of the serious damage caused by excessive heating (Rakov and Uman 1990). For instance, it is generally assumed that the majority of lightning-caused wildfires result from lightning with LCC (Fuquay et al. 1967, 1972). Although Fuquay et al. (1972) did not rule out the possibility that lightning flashes that do not have an LCC phase can ignite a wildfire, they did find that of 11 forest fires examined, all 11 were ignited by lightning with an LCC phase. Therefore, it appears that an LCC phase may be a necessary condition for fire ignition. On the other hand, two of the 13 lightning flashes that had an LCC phase, 15.4 percent, did not ignite a fire.

From the analyses of 14 lightning flashes in New Mexico with continuing current, it was found that the average current was 184 amperes and the average duration was 184 milliseconds (Williams and Brook 1963). Approximately 50 percent of all lightning flashes contain an LCC component (Uman 1987). This is corroborated by Fuquay et al. (1967) who found that about half of 856 lightning flashes in Montana had LCC. However, this fraction may differ substantially between flashes that have a negative or positive charge to the ground. According to Anderson (2002), approximately 20 percent of negative lightning flashes and 85 percent of positive flashes have an LCC.

The polarity of lightning, negative or positive, is typically associated with lightning from different sources and with different characteristics (Uman 1987). Negatively charged lightning flashes typically originate as a downward-moving negatively charged leader from the lower extremities of a cloud. The result is a lowering of negative charge to the earth. Worldwide, approximately 90 percent of all cloud-to-ground flashes are negatively charged (Rakov and Uman 2003). Positive lightning events account for less than 10 percent of all lighting worldwide (Uman 1987). Positive discharges to the earth from lightning flashes typically originate in the upper extremities of clouds, and particularly when the anvil is horizontally separated from the rest of the cloud. Although less common overall than negative lightning events, positive lightning has been associated with the largest recorded lightning currents, those ranging from 200 kiloamperes to 300 kiloamperes. In general, positive lightning flashes typically transfer much more charge to the earth than negative flashes.

The ratio of positive to negative lightning flashes may not be constant. For instance, the proportion of lightning events that have a positive charge may increase with the elevation above sea level (Lewis and Foust 1945). They observed 2721 ground flashes and 18 percent overall were positively charged. However, the percentage of positive flashes ranged from 3 percent near sea level to 30 percent in the mountains of Colorado, at elevations from approximately 2000 meters (6562 feet) to 4000 meters (13123 feet). In addition, the proportion of all lightning flashes that are positively charged has been observed to increase towards the end of individual thunderstorms (Orville et al. 1983). Moreover, this proportion is the least (a few percent) during the summer months and greatest (about 80 percent) during thunderstorms that occur during the winter months (Orville et al. 1987). On the other hand, Rakov and Uman (1990) compared the characteristics of negative flashes from Florida and New Mexico and found that the proportion of flash types was generally similar regardless of location.

In one study that attempted to document the proportion of positively charged lightning flashes that were associated with LCC, Fuquay (1982) monitored lightning over a three-year period and found that approximately 3 percent of all the flashes were positive. From the resulting 75 positive lightning flashes in Fuquay's data set, 40 had continuing current that was greater than 40 milliseconds. Of the remaining 18 flashes, at least one continuing current phase was observed in each case, but the duration of these discharges ranged from 5 milliseconds to less than 40 milliseconds. Nevertheless, from this small sample, it can be estimated that about 53.3 percent of positive flashes contain at least one LCC episode and are thus able to ignite a wildfire.

Detection and sensing of lightning in Florida over a nine-year period were used to characterize LCC in negatively charged lightning flashes to the ground (Rakov and Uman 1990). Of a total of

141 flashes, 57 or 40.4 percent had LCC. Several additional studies were referenced and included in the analysis by Rakov and Uman (1990), but it is unclear if the data from these outside investigators are limited to negative lightning events. Nevertheless, if these additional data are included, a total of 346 lightning flashes were represented with 152 or 43.9 percent containing LCC.

The conclusion that LCC is a primary controlling factor in lightning-caused fires appears to be widely accepted (Rakov and Uman 1990, Anderson 2002). However, an alternate opinion was proposed by Larjavaara et al. (2005). They examined the probability of igniting a lightning-caused fire based on the intensity of the lightning flash. They concluded that positive and negative strokes ignite fire with equal probability, approximately 11 percent. For both polarities, ignition probabilities were very low for strokes below 3 kiloamperes. These probabilities increase to about 0.00015 at strength levels of about 8 kiloamperes. The probabilities remain constant for negative strokes up to 100 kiloamperes. For positive strokes, the probabilities continue to increase to approximately 0.0013 at about 90 kiloamperes.

Probability of lightning with long continuing current

To model the probability of at least one LCC (p_{LCC}), we estimated the proportion of lightning flashes with characteristics suitable for igniting wildfires. To accomplish this, we assume that 53 percent of positive lightning cloud-to-ground strokes had LCC and therefore could ignite wildfires. We also assume that 44 percent of negative flashes have LCC. Then for each subseason, we assume that the number (n) of lightning flashes in each pixel in a given year follows a Poisson distribution. Note that if the presence of a flash in one time interval does not influence the probability of a flash in another non-overlapping time interval, the assumption of independence among Poisson observations in non-overlapping time intervals will be supported. The derivations of our version of p_{LCC} are as follows.

We wish to approximate the expression of the probability of at least one LCC from a flash of a particular type in a time period,

$$\sum_n (1-r^n)P(n) \ ,$$

where $r = 1-0.53 = 0.47$ for positive flashes and $r = 0.56$ for negative flashes. If we can assume that the number of flashes per time period has a Poisson distribution,

$$P(n) = \frac{e^{-\lambda}\lambda^n}{n!},$$

where λ is the average number of flashes per time period, we have

$$\sum_n (1-r^n)P(n) = 1-\sum_n r^n P(n) = 1-\sum_n r^n \frac{e^{-\lambda}\lambda^n}{n!} = 1-e^{-\lambda}\sum_n \frac{(r\lambda)^n}{n!} = 1-e^{-\lambda}e^{r\lambda}\sum_n \frac{e^{-r\lambda}(r\lambda)^n}{n!}$$
$$= 1-e^{-\lambda}e^{r\lambda} = 1-e^{-\lambda(1-r)}.$$

For example, suppose that the average number of positive flashes is $\lambda = 4.2$ for a period of 21 days, then an estimate of the probability of at least one LCC from a positive flash in this period is

$$1 - e^{-\lambda(1-r)} = 1 - e^{-4.2 \times 0.53} = 0.8920.$$

If the average number of negative flashes is 2.9, then the probability of at least one LCC from a negative flash is

$$1 - e^{-\lambda(1-r)} = 1 - e^{-2.9 \times 0.44} = 0.7208.$$

This Poisson model approach described above was incorporated into the geographic information system by calculating the density of lightning flashes for each time period and polarity using the kernel method of the ArcGIS Spatial Analyst Density Function (ESRI 2004). A search radius of 4 square kilometers was used and density of lightning flashes was expressed as number per square kilometer. Thus, we used a search radius that was four times as large as our output units. Density was calculated for the entire data set of lightning flashes and then clipped to our study area boundary, which was the geographical extent of the land cover map (McKown et al. 2003). Average density for each pixel was then calculated by dividing the density by the number of years represented by the lightning data set (seven).

Probability of ignition from a suitable lightning flash

Assuming that a suitable lightning flash has occurred, the potential for a wildfire to be ignited to the level of at least a smoldering state is determined by the characteristics of the lightning flash, fuel conditions, and moisture levels (Anderson 2002). A method for expressing this potential in terms of probabilities was developed by Latham and Schlieter (1989). We adapted this method with some modifications.

Latham and Schlieter (1989) subjected several different types of fuels to discharges from an electric arc that simulated lightning with continuing current. The probabilities of ignition from these discharges, under moisture conditions that range from 0 to 40 percent, were modeled for both positive and negative lightning flashes using logistic regression. Four of these models were incorporated into this project by ranking them from very low to high ignitability for conditions that commonly occur in the Los Alamos region (Table 4). We assumed further that open water, paved areas, bare rock, and similar land cover conditions would not be ignitable by lightning and added a fifth condition with zero probability that an ignition would occur. One of the five ignitability classes and the associated equations were then assigned to each of the land cover classes that make up the regional land cover map (Table 5).

Table 4. Ignition probability models used in this study (M = fuel moisture).

Fuel type	Ignitability	Negative flash	Positive flash
Open water, bare rock, pavement, etc.	None	0	0
Punky wood (rotten chunky)	Very low	0.59*exp(-0.094*M)	0.44*exp(-0.11*M)
Commercial peat moss	Low	0.84*exp(-0.06*M)	0.71*exp(-0.07*M)
Engelmann spruce duff	Moderate	0.8-0.014*M	0.62*exp(-0.05*M)
Ponderosa pine litter	High	1.04*exp(-0.054*M)	0.92*exp(-0.087*M)

Table 5. Assignment of ignition probability equations to land cover classes.

		Ignitability				
Class number	**Cover class**	**None**	**Very low**	**Low**	**Moderate**	**High**
29	RONE Shrubland				X	
16	PIED-JUMO/Sparse-Rock Woodland		X			
14	PIED-JUMO/Sparse-Soil Woodland		X			
25	POTR Shrubland			X		
7	Open water	X				
9	Riparian-Wetland		X			
32	Urban, Paved	X				
31	Urban, Vegetated		X			
18	PIED-JUMO/ARTR Woodland			X		
26	POTR Forest				X	
2	Montane Grassland					X
20	BRCA-AGTR Grassland				X	
19	PIED-JUMO/BOER Wooded Grassland			X		
3	ABCO-PSME Woodland					X
30	PIED Forest				X	
27	PIPO/Other grass Woodland					X
6	Sparse-Bare soil		X			
13	QUGA Shrubland				X	
5	Evergreen-POTR Forest					X
10	Sparse-Bare Rock		X			
24	ABLA-PIEN Forest				X	
17	Other Shrubland				X	
12	PIPO/BOGR-SCSC Woodland				X	
28	JUMO Wooded Grassland			X		
23	PIPO/QUGA Woodland					X
15	Submontane Grassland					X
1	Valles Caldera Grassland					X
21	PIPO Forest					X
11	PIED-JUMO/BOGR Woodland				X	
4	ABCO-PSME Forest					X

We assumed that the percent fuel moistures of Latham and Schlieter (1989) are suitably represented by the equilibrium moisture contents (EMC) of wood (Simpson 1998). The EMC depends on the temperature (degrees Fahrenheit) and relative humidity (percent) according to the following equation:

$$EMC = \frac{1800}{W}\left(\frac{Kh}{1-Kh} + \frac{K_1Kh + 2K_1K_2K^2h^2}{1+K_1Kh+K_1K_2K^2h^2}\right),$$

where
EMC = the equilibrium moisture content (percent) and
h = the relative humidity (percent/100).

The coefficients of absorption (W, K, K_1 and K_2) used in the EMC approximation developed by Simpson (1998) were originally established by Hailwood and Horrobin (1946) as follows:

$$W = 330 + 0.452T + 0.00415T^2$$

$$K = 0.791 + 0.000463T - 0.000000844T^2$$

$$K_1 = 6.34 + 0.000775T - 0.0000935T^2$$

$$K_2 = 1.09 + 0.0284T - 0.0000904T^2$$

where
T = temperature (degrees Fahrenheit).

We used data collected from 1998 to 2004 at the TA-6, TA-49, TA-53, TA-54, and Pajarito Mountain weather towers to model the temperature and relative humidity inputs required by the EMC relationship developed by Simpson (1998). First, we used the known linear relationship with changes in elevation to model temperatures (Stull 2000). The daily maximum temperature records over the seven-year period were averaged to give an average maximum temperature for each calendar day and at each of the five weather towers. Missing data for any day at any of the weather towers resulted in the deletion of that day-tower from further analysis. For the surviving data, an average was computed for each of the subseasons at each of the towers. Then, the average maximum temperature over all weather stations was regressed against the elevation at each station, by subseason.

Second, this process was repeated for the minimum daily relative humidity record. The regression coefficients for each of the temperature and relative humidity models are shown in Table 6. The results are also graphed for temperature (Figure 7) and relative humidity (Figure 8). These regression models were used to calculate temperature and relative humidity for each elevation grid cell in the land cover map. A 10-meter digital elevation model was resampled to the 50-foot grid cell sizes that correspond to the land cover map and used for this purpose.

Table 6. Regression coefficients for modeling maximum temperature and relative humidity from elevation.

	Maximum temperature		Relative humidity	
Subseason	**Intercept**	**Slope**	**Intercept**	**Slope**
1	88.7	-0.0044	0.9890	0.0043
2	101.1	-0.0047	0.9972	0.0034
3	112.7	-0.0047	0.9854	0.0021
4	116.4	-0.0046	0.9939	0.0027
5	116.3	-0.0047	0.9972	0.0040
6	109.8	-0.0047	0.9962	0.0037

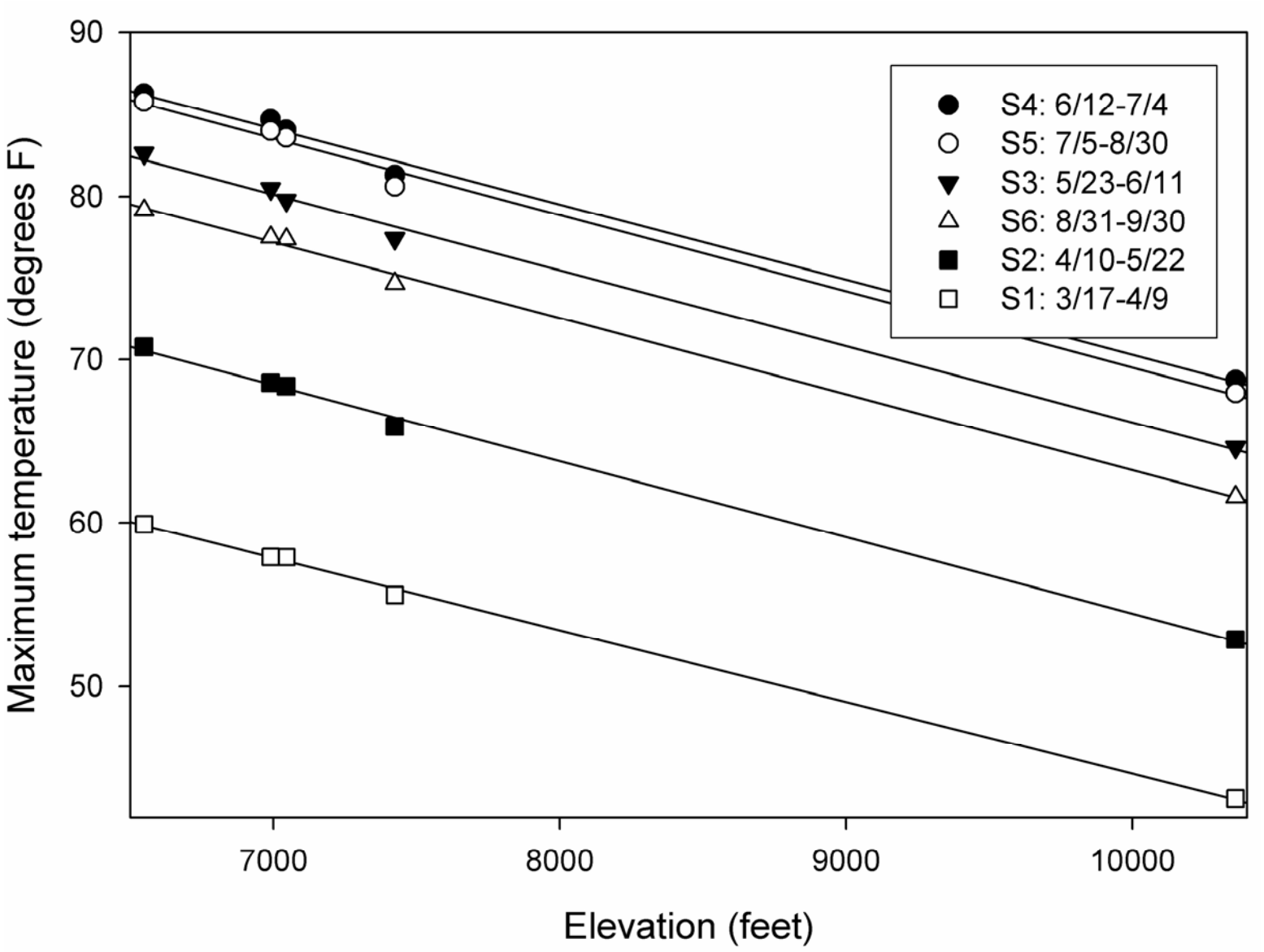

Figure 7. Maximum temperature versus elevation, by subseason

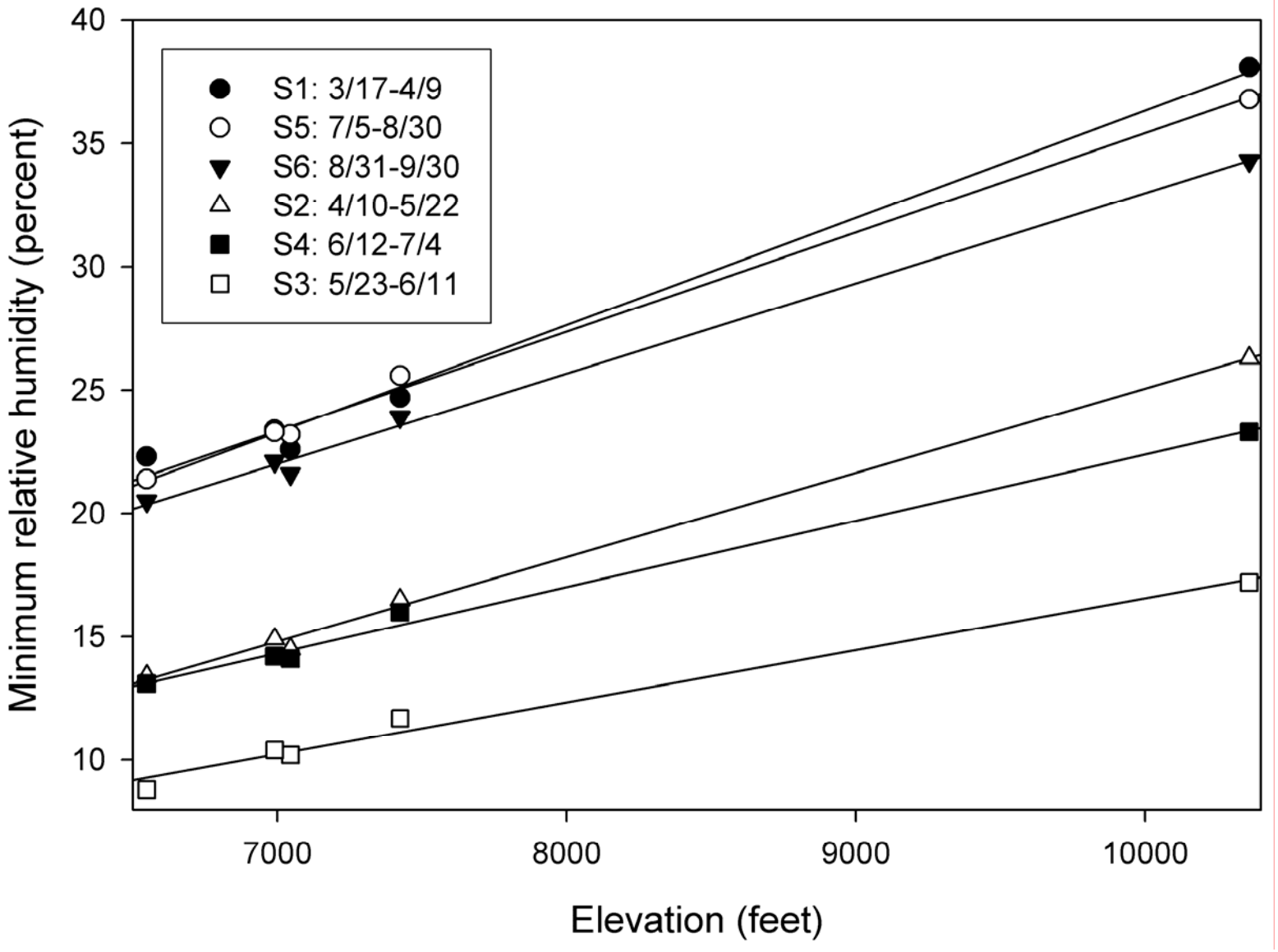

Figure 8. Minimum relative humidity versus elevation, by subseason.

Rainfall effects on the probability of ignition

The first two terms incorporated into the overall probability model of wildfire risk assume that a suitable lightning flash may occur (p_{LCC}) and that ignition into at least a smolder state may result in a receptive fuel (p_{ign}). The first term, p_{LCC} , incorporates specific characteristics of the lightning flash and p_{ign} incorporates fuel type and EMC, which is determined by average temperature and average relative humidity over the course of a subseason.

While EMC is an acceptable method to estimate equilibrium moisture content for an entire subseason, it does not consider short-term changes in moisture levels that occur with precipitation that is often associated with lightning flashes. The occurrence of precipitation shortly before a lightning flash will wet the fuels and temporarily decrease their potential for ignition. Fine fuels are highly sensitive to wetting by rainfall. Fosberg (1972) found that the most important factor causing an increase in fuel moisture is not the amount of rainfall but rather the duration of time (*T*) that the fine fuels have been wet at the surface before the occurrence of lightning. The fuel absorbs the moisture at the surface, thereby increasing the fuel moisture exponentially in time toward a saturation value of 76 percent. Fuquay et al. (1979) adapted this approach as follows:

$$EMC_f = EMC_i + (76 - EMC_i) * (1 - \gamma e^{-T/\tau}) \quad ,$$

where

EMC_f = the final, corrected equilibrium fuel moisture,

EMC_i = the initial equilibrium fuel moisture calculated from Simpson (1998),

γ = a parameter that varies with the fuel type (in this case, equal to one),

τ = time-lag for the fuel type (in this case, one-hour), and

T = the time period from the beginning of a significant rainfall event until a lightning flash.

To make the correction to EMC, we need only the EMC before correction and the time (*T*) that the fine fuels are wet. We attempt to determine a representative value of *T* by comparing records of rainfall at the TA-6 weather station with lightning that has struck the ground in the proximity of TA-6. Since rainfall can vary strongly from one station to the next even when the two are separated by as little as 10 kilometers, we try to keep the area around TA-6 for enumerating lightning flashes as small as possible. For the most active lightning subseason, July 5 through August 30, for example, we count all lightning flashes within 1/100 of one degree in all four directions from TA-6. This is an area of about 4 square kilometers centered on TA-6. Over the years 1994 through 1999, 52 cloud-to-ground flashes are counted in this area during this subseason.

Once every 15 minutes, rain that has been collected over the past 15 minutes is tallied and the information is recorded at the TA-6 weather tower. Therefore, the exact time that any rain falls is unknown. Only the count for every 15-minute period is known. For this reason, the exact time of the lightning flash is rounded forward to the nearest quarter of an hour. This affords a more ideal comparison of time of lightning and rainfall. A flash at 7:03, for example, is considered to have been counted at 7:15, just as rain at 7:03 would be counted at 7:15.

The time of each flash near TA-6 is compared to times of rainfall there. If rain was counted at 6:15 and lightning was counted at 7:15, for example, then the time *T* that the fuels were wet is one hour, for that particular lightning flash. If rain was counted after the time of the lightning flash, or not at all, the fuels were considered to be dry and *T* is set to 0. In a number of cases, rain was counted at the same time as the lightning flash. In half of those cases, we assume that the rain fell before the lightning and we consider *p* to be 7.5 minutes. In the other half of cases that rain and lightning are counted simultaneously, we assume that the rain fell after the lightning flash and the fuel is dry ($T = 0$).

For all six subseasons, we minimize the area around TA-6 in which we count lightning flashes while keeping the sample size of flashes to be about 40 to 50. One exception is the first fire subseason (March 17–April 9). During that time period, only 13 flashes in an area of approximately 100 square kilometers centered on TA-6 were counted. Nonetheless, we chose not to increase the counting area to get more flashes.

The latitude and longitude of the boundaries of the areas for counting lightning flashes, as well as the approximate size of areas for counting, vary (Table 7). However, this maximizes the number of flashes that can be used to calculate *T*, the median duration of wetness in hours.

Table 7. Intermediate and final correction of the equilibrium moisture content (EMC).

Wilfire Subseason	Longitude boundaries of flash count area (degrees west)	Latitude boundaries of flash count area (degrees north)	Approximate area of flash count area (sq. km)	Number of lightning flashes counted (1994–1999)	Median duration of wetness *T* (hours)
S1: Mar 17 – Apr 9	-106.**26**96, -106.**36**96	35.**91**14, 35.**81**14	100	13	0
S2: Apr 10 – May 22	-106.**27**96, -106.**35**96	35.**90**14, 35.**82**14	64	38	0.125
S3: May 23 – June 11	-106.**28**96, -106.**34**96	35.**89**14, 35.**83**14	36	51	0.125
S4: June 12 – July 4	-106.**29**96, -106.**33**96	35.**88**14, 35.**84**14	16	44	0
S5: July 5 – Aug 30	-106.**30**96, -106.**32**96	35.**87**14, 35.**85**14	4	52	0.125
S6: Aug 31 – Sep 30	-106.**29**96, -106.**33**96	35.**88**14, 35.**84**14	16	55	0.25

The durations of wetness (*T*) within each subseason were quite skewed, with sample sizes ranging from 13 to 55. Most values were near zero and a few values ranged from four to 24 hours. This skew resulted in mean values of *T* that were not representative of wetness duration within the subseason. Therefore, we estimated wetness duration as the median of the sample for each subseason rather than the mean value.

Probability of survival following successful ignition

To construct p_{sur} , we assumed that if a lightning-ignited fire survives in a smolder state for two days or more it will certainly result in a wildfire. On the other hand, it is assumed that a precipitation event that occurs within two days has a significant chance to extinguish the smoldering fire. Given these assumptions, we begin by estimating the probability of precipitation during any given two-day period, which we call p_{rain} . First we calculate number of days during which precipitation is observed divided by the total number of days in the subseason ($freq_{rain}$). Then, p_{rain} is determined as

$$p_{rain} = 1-(1- freq_{rain})*(1- freq_{rain}) = 2* freq_{rain} - freq_{rain}^{2} .$$

We used rainfall from the Los Alamos archive during the period 1945 to 2004 (50 years) to calculate p_{rain} for each wildfire subseason.

In addition, we wish to account for the fact that some rains are heavier than others. Precipitation during heavy rainfall events is more likely to extinguish a smoldering fire than precipitation during light rainfall events. To account for this, we define a weighting factor W_{rain} to reflect the relative amounts of rainfall that might fall in a typical rainstorm for each subseason. We do this by calculating *P*, the total amount of precipitation during a wildfire subseason divided by the number of days in that subseason in which rainfall was observed. *P* is the average amount of rainfall on a rainy day in each subseason. Then, *P* is normalized by calculating W_{rain} for each subseason, as follows

$$W_{rain,i} = \frac{P_i}{P_{greatest}},$$

where
i = 1,…,6.

The largest value for W_{rain} is equal to unity and the remaining five values are proportionally less. Next, W_{rain} and p_{rain} are used to calculate p_{sur} , as the probability of not having a heavy rain in a two-day period.

$$p_{sur} = 1-W_{rain}\,p_{rain}$$

The intermediate and final results of these calculations are given in Table 8.

Table 8. Intermediate and final calculations for probability of survival.

Subseason	p_{rain}	*P*	W_{rain}	$1-W_{rain}p_{rain}$
1	0.379	0.151	0.649	0.754
2	0.360	0.181	0.778	0.720
3	0.419	0.189	0.810	0.661
4	0.419	0.178	0.764	0.680
5	0.729	0.233	1	0.271
6	0.477	0.200	0.860	0.590

Calculation of wildfire risk

The intermediate calculations of the probability of lightning with LCC (p_{LCC}), the probability of ignition (p_{ign}), and the probability of survival (p_{sur}) were used to calculate the probability of a lightning-ignited fire ($p_{fire}(s)$) for a particular subseason. Since intermediate probabilities were calculated for both negative and positive lightning flashes, the final probability was calculated for each pixel in the land cover map using the union between two independent events, as follows:

$$p_{fire}(s) = p_{LCC^+} p_{ign^+} p_{surv^+} + p_{LCC^-} p_{ign^-} p_{surv^-} - p_{LCC^+} p_{ign^+} p_{surv^+} * p_{LCC^-} p_{ign^-} p_{surv^-}$$

where

$p_{LCC^+} p_{ign^+} p_{surv^+}$ = the joint probability of a wildfire ignition from a positive lightning flash and

$p_{LCC^-} p_{ign^-} p_{surv^+}$ = the joint probability of a wildfire ignition from a negative lightning flash.

This calculation was repeated for each of the subseasons (s_i) to estimate $p_{fire}(s_i)$, i = 1,…,6. In addition, to provide for an overall assessment of wildfire risks throughout the fire season in the Los Alamos region ($p_{fire}(S)$), the final subseason values of the probability of lightning-ignited fire were combined according to

$$p_{fire}(S) = 1 - \prod_{i=1}^{6} (1 - p_{fire}(s_i)) .$$

This final value ($p_{fire}(S)$) may be interpreted as the risk of experiencing at least one fire during the entire fire season (S) that was ignited by lightning and smolders in the litter and duff for up to two days.

Results

The spatial distributions of the final probabilities of wildfire risk were mapped for each of the six subseasons (Figure 9a–f). To facilitate comparison between subseasons, a constant scale of wildfire probability was used.

The first subseason (S1: March 17 to April 9) has the least amount of wildfire risk in terms of the probability of lightning-ignited fires (Figure 9a). Much of the area results in zero probability. The highest probability of a wildfire ignition is 0.04. The greatest tendencies for these types of fires to occur are concentrated along the lower-elevation areas on the eastern and southern flanks of the Jemez Mountains, including LANL.

The second subseason (S2: April 10 to May 22) generally results in higher probabilities of a wildfire, up to a maximum of 0.13, with only small areas containing probabilities approaching zero (Figure 9b). The highest probabilities tend to occur in the higher mountainous segments of the region and along the boundaries of Los Alamos County. The probabilities on LANL property are mostly 0.06 or less.

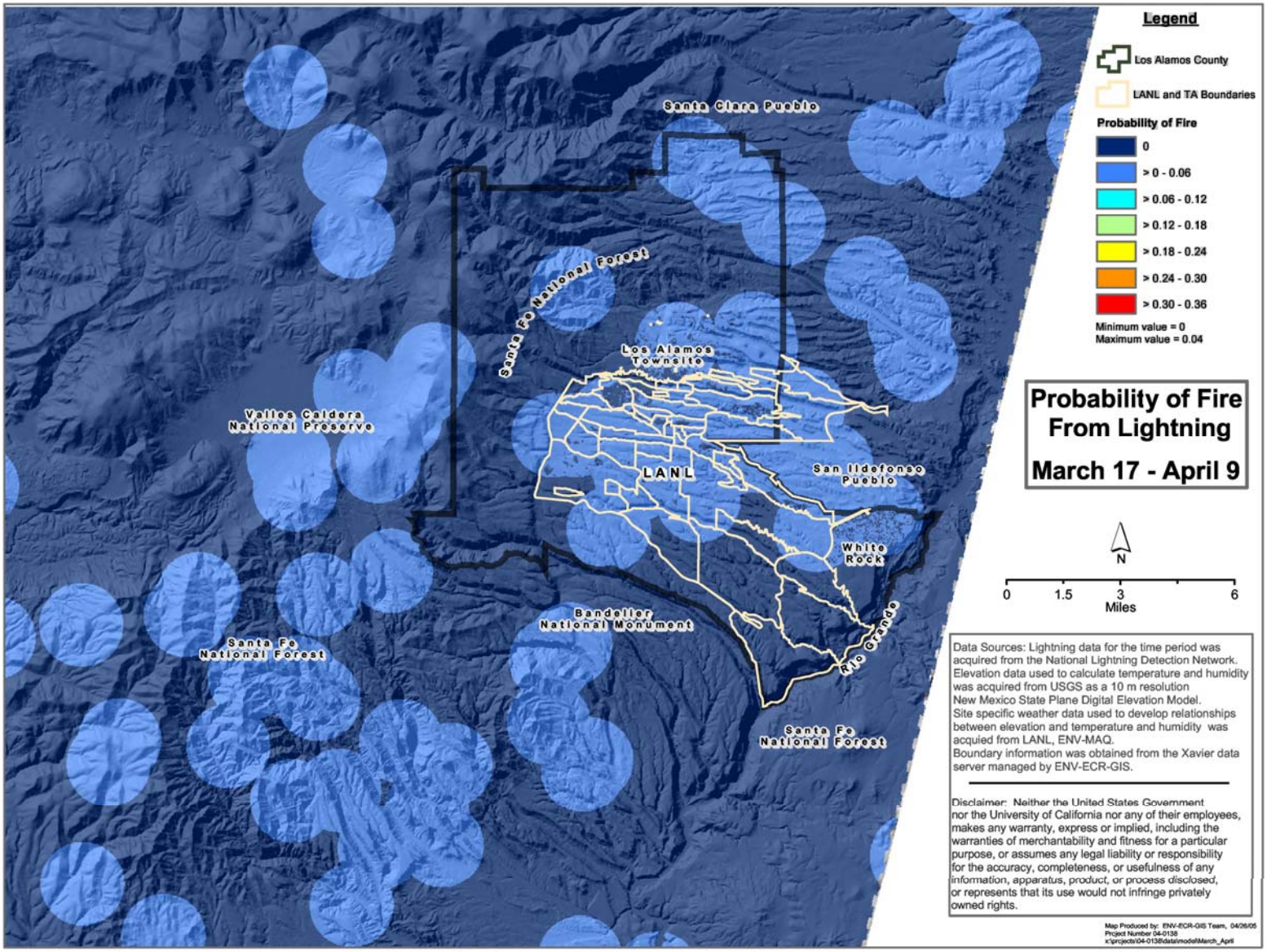

Figure 9a. Probability of fire from lightning (S1: March 17 to April 9).

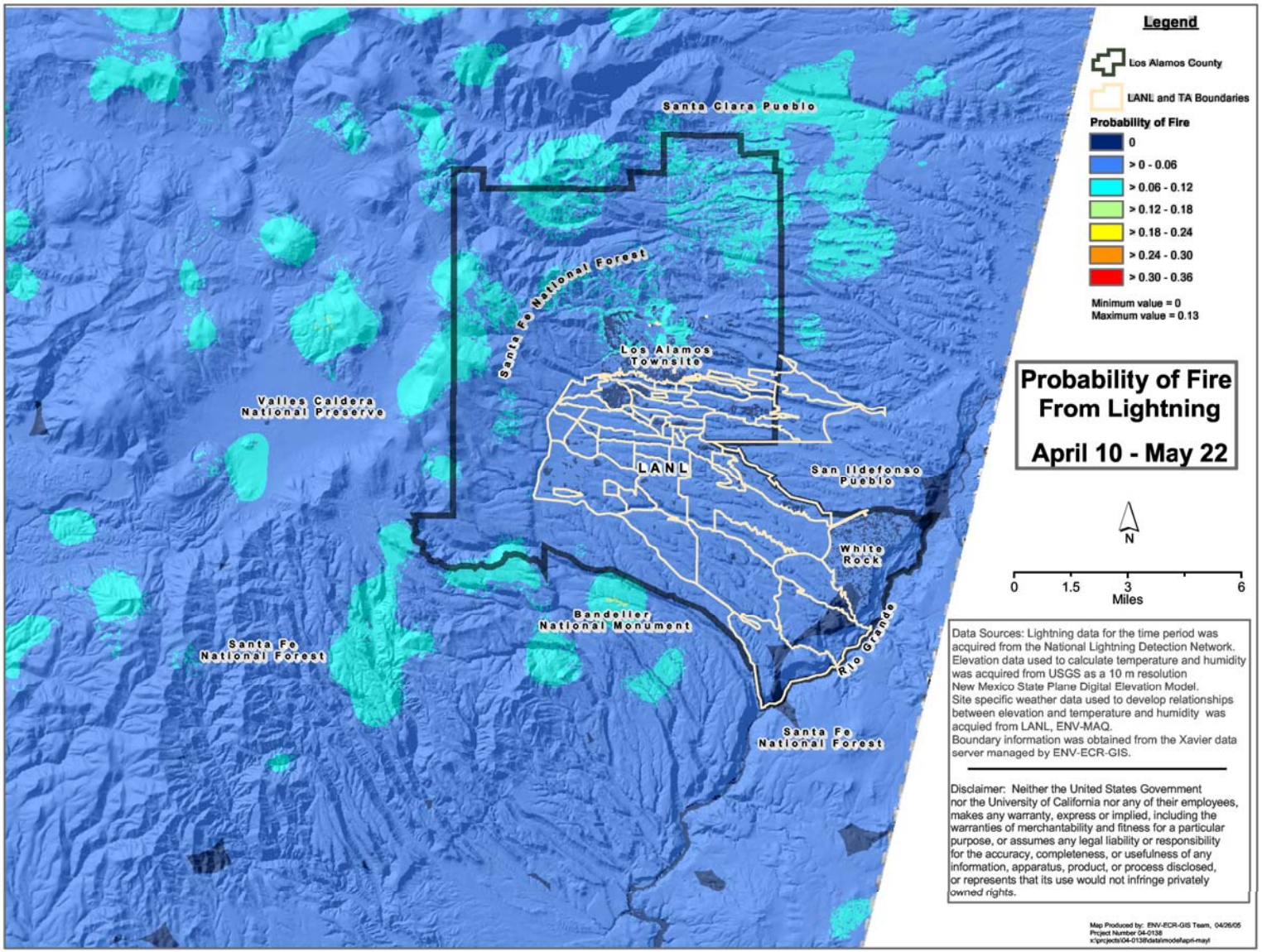

Figure 9b. Probability of fire from lightning (S2: April 10 to May 22).

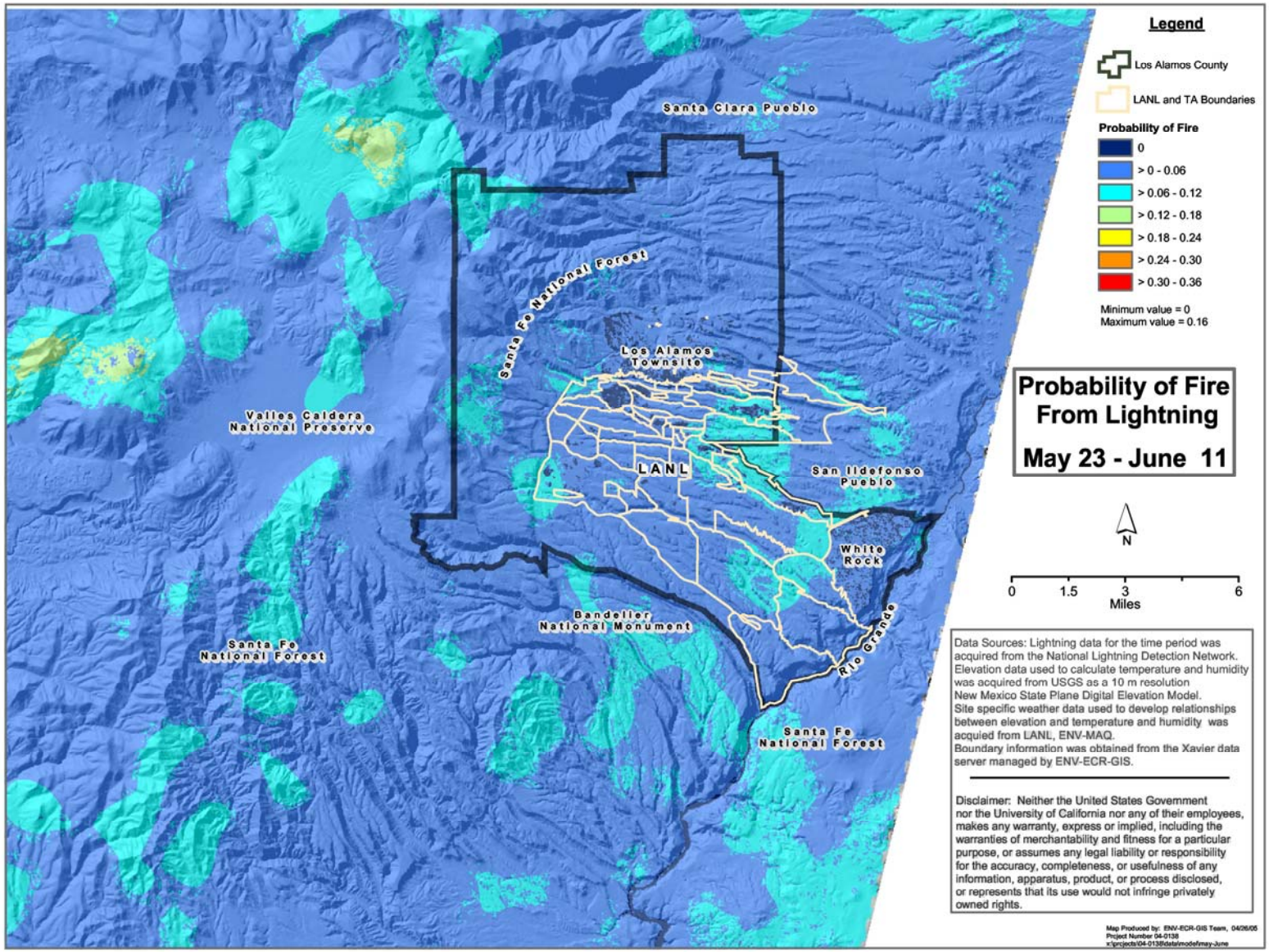

Figure 9c. Probability of fire from lightning (S3: May 23 to June 11).

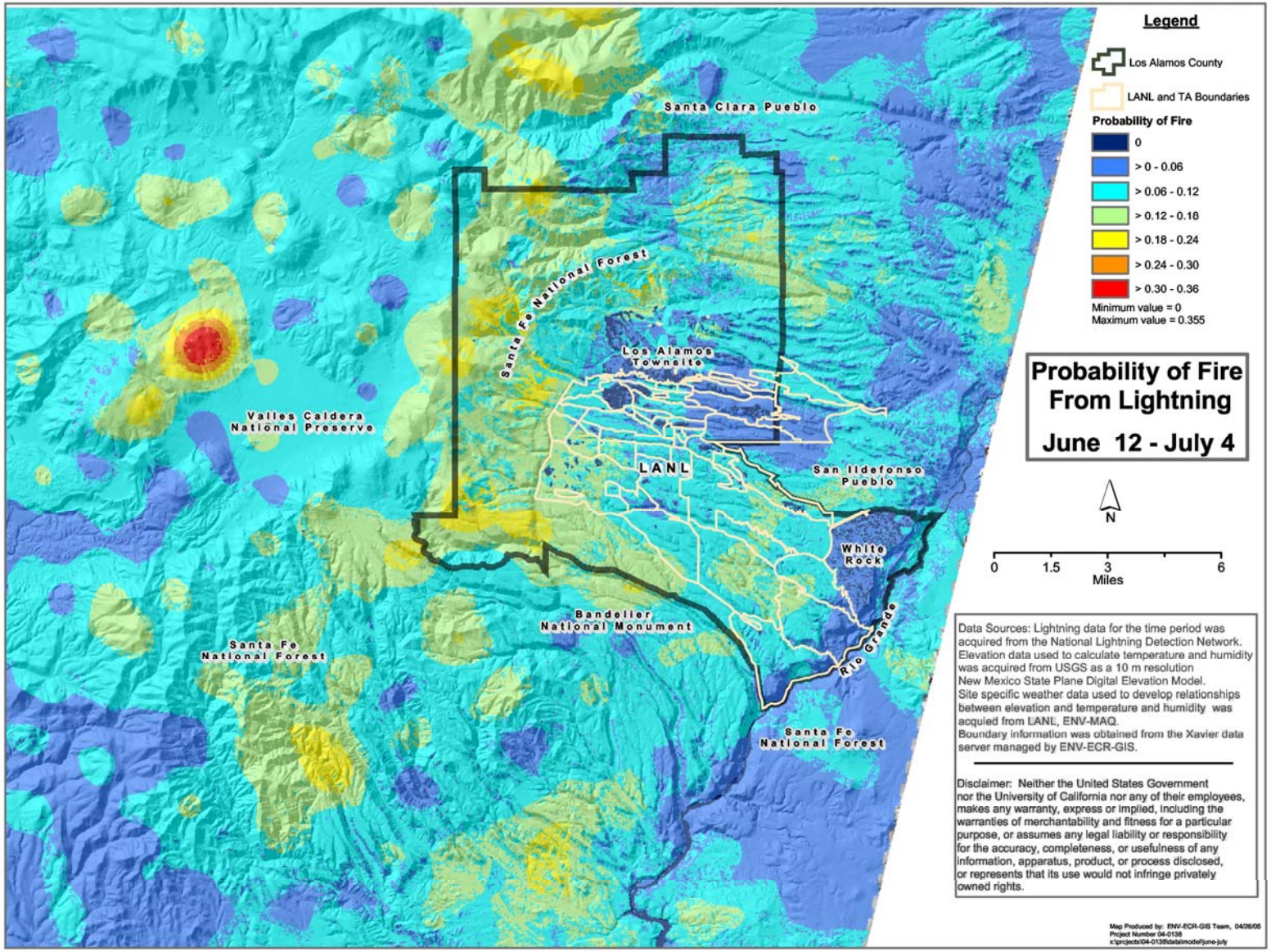

Figure 9d. Probability of fire from lightning (S4: June 12 to July 4).

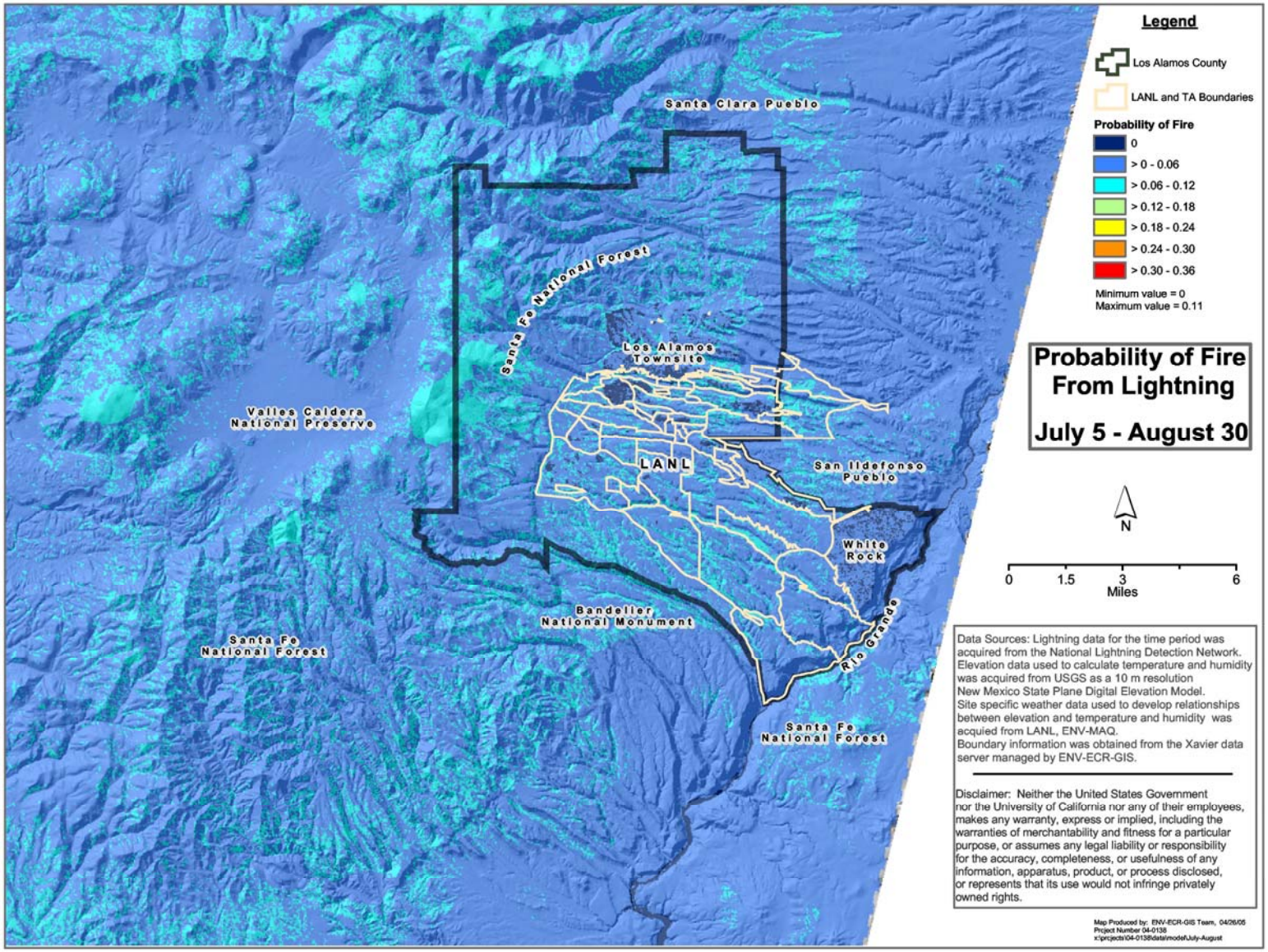

Figure 9e. Probability of fire from lightning (S5: July 5 to August 30).

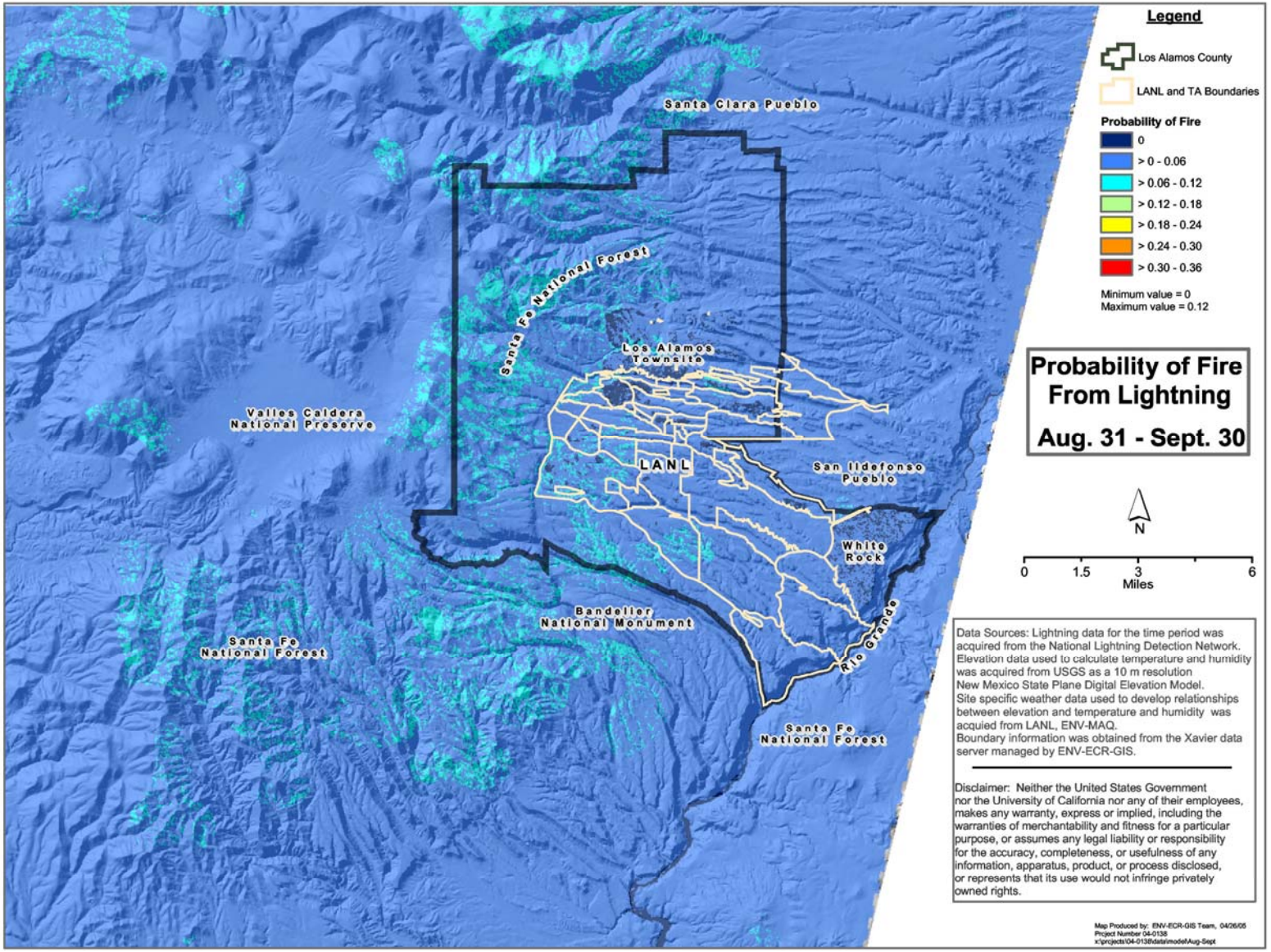

Figure 9f. Probability of fire from lightning (S6: August 31 to September 30).

The probabilities of the third subseason (S3: May 23 to June 11) are qualitatively similar to those of the second subseason, although the highest probabilities, up to 0.16, have a greater tendency to be concentrated in the mountainous areas in the Valles Caldera region to the northwest of Los Alamos (Figure 9c). Probabilities at LANL are mostly less than 0.06, although they increase in the selected portions of LANL property and in the adjacent mountains to as high as 0.12 during the third subseason.

With the fourth subseason (S4: June 12 to July 4), the probabilities are greater than the probabilities for any of the other subseasons (Figure 9d). The wildfire risks increase to 0.355 in one small portion of the study area, west of the Headquarters at the Valles Caldera National Preserve. In contrast, the wildfire risk for most of the region is 0.18 or less. At LANL, the highest probabilities never exceed 0.18, but increased to a maximum of 0.24 to the northwest and the southwest of LANL property.

The wildfire risk for the fifth subseason (S5: July 5 to August 30) is reduced relative to that of the previous subseason (Figure 9e). A maximum risk of 0.11 is observed for S5, which is the monsoon time period. The risks throughout LANL are uniformly distributed. However, two large areas of higher probabilities, between 0.06 and 0.11, are observed in the Sierra de los Valles from Cerro Grande to the Pajarito Mountain and in the Redondo Peak area.

The wildfire risks of the sixth subseason (S6: August 31 to September 30) remain low, at 0.12 or less. The highest concentrations of risk, ranging from 0.06 to 0.12, occur in the Sierra de los Valles and in the adjacent plateaus (Figure 9f). This includes much of the western portions of LANL and the mountainous region to the west extending to Pajarito Mountain and the Cerro Grande.

The averaged probabilities over the entire fire season for the Los Alamos region are shown in Figure 10. The largest average probability over the entire fire season, 0.49, occurs in the Sierra de los Valles to the west of Los Alamos and in the Valles Caldera area. The probabilities of a wildfire occurring throughout much of LANL are 0.26, or less. However, the probabilities of the western portions of LANL increase to a maximum of 0.36. In the mountains immediately to the west of LANL, typical probabilities of wildfire ignitions increase to the 0.27 to 0.45 range. In contrast, sections of the Sierra de los Valles that were burned at high severities exhibit lower probabilities, which typically range from 0.09 to 0.18.

Discussion

These results of this modeling effort are valid for a specific set of circumstances. The values for $p_{fire}(t)$ can be interpreted as the potential for a suitable lightning flash to occur, cause an ignition in receptive litter and duff fuels, and for this fire to continue in a smoldering state for at least two days. Ignitions of this sort are not uncommon in the Los Alamos region. Typically, these ignitions self-extinguish or are suppressed by emergency management personnel. To increase the overall relevance of this model, additional terms should be added to the modeling system that represent continued burning of these smoldering fires to a flaming state, to the nearby grasses and forbs, to the shrub canopy and ladder fuels, and to the overstory canopy.

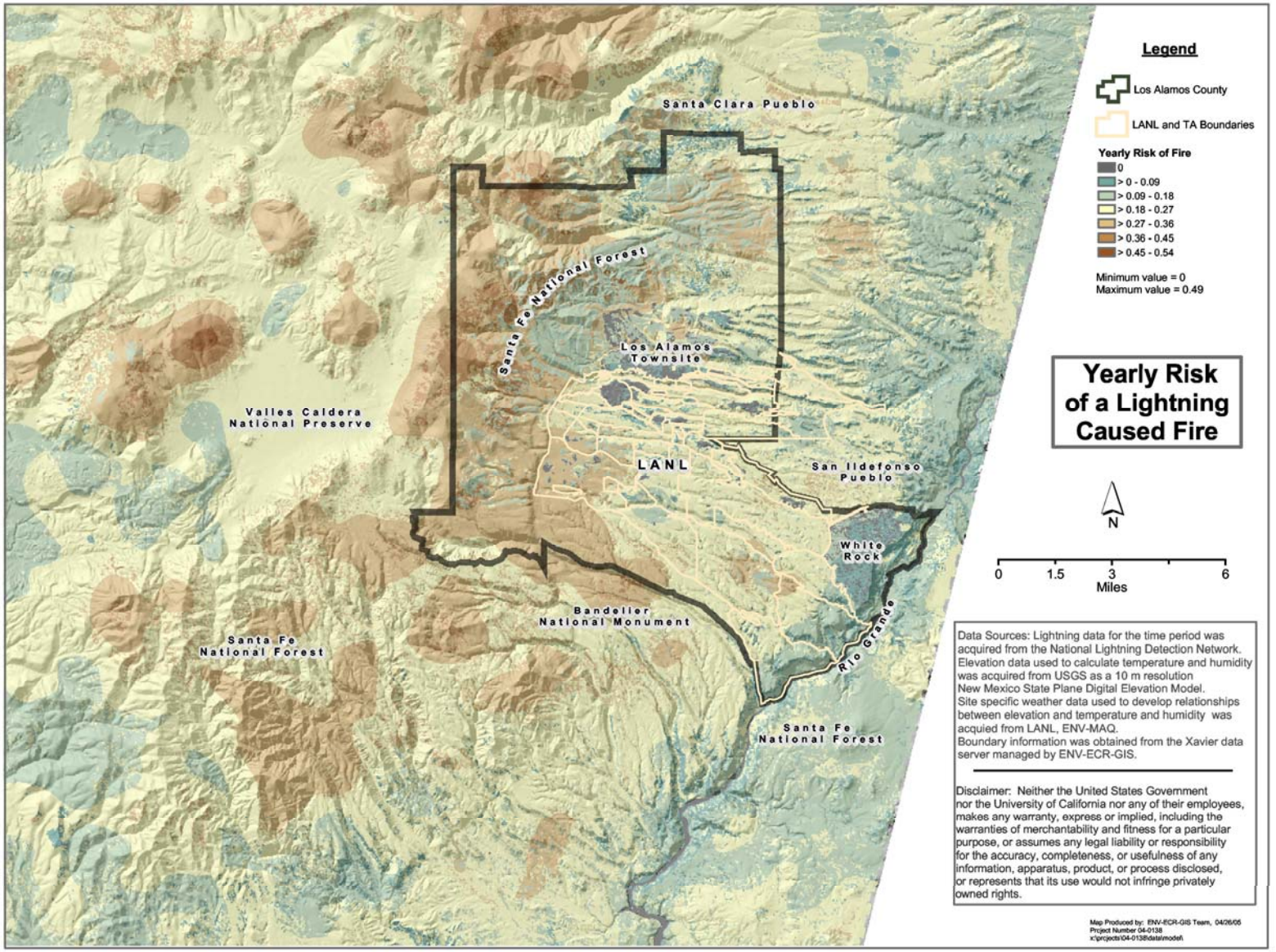

Figure 10. Average risk of lightning-caused fire over the entire wildfire season (March 17 to September 30).

Additional sources of ignitions, such as humans, should also be considered as separate modeling components.

The potential for ignition in receptive fuels (p_{ign}) is modeled under the assumption that ignitions will occur in the litter and duff. These types of fuels occur at the soil surface and are not readily amenable to reduction through commonly applied management activities to reduce the fire hazards, such as thinning and overstory removal. Therefore, the current version of the model is not sensitive to changes in overstory structures resulting from thinning and other similar fire hazard reduction treatments. On the other hand, the model outputs are very sensitive to changes in litter and duff levels. This is evidenced by the low fire risk in the areas to the northwest of Los Alamos that were severely burned in the Cerro Grande Fire, including a total removal of the litter and duff layers (see Figure 10).

The results of this project appear to corroborate previous conclusions that the primary risk to LANL from wildfire emanates from the western and southwestern portions of the Laboratory and in the adjacent mountains to the west (Balice et al. 1999, U.S. Department of Energy 1999). The fuel levels are greater in mountainous areas with ponderosa pine and mixed conifer forests, the winds during the fire season originate from the south and the southwest, and the density of lightning flashes is greater at higher elevations. This leads to the management implication that facilities at the southwestern portion of LANL are at the greatest risk from wildfire, on a relative basis. Facilities along the western and northern perimeter of LANL and throughout the central portions of LANL are also at a higher relative risk from wildfire, depending on the subseason and the distribution of lightning flashes.

The results of the current project compare well with those of the 1999 LANL Site-wide Environmental Impact Statement (U.S. Department of Energy 1999). In the earlier analysis, it was concluded that there was a one-in-ten chance that wildfire would be ignited, would survive, and that a major wildfire would burn to the boundary of LANL in any given year. This conclusion assumes many more steps in the sequence of events. In the current project, we only include the first three steps related to the occurrence of a suitable lightning event, the heating of a suitable fuel to the point of ignition or smoldering, and the potential for rainfall to extinguish the smoldering fire. One might conclude that these results imply that wildfire risks have been reduced at LANL in the intervening five years. However, since contrasting methods were used in the two projects, any comparisons between 1999 and the present can only be tentative.

The current project is a first attempt to develop probability models for determining risks to LANL from wildfire. The explicit temporal-spatial nature of the current results, which allow for comparisons in time and space, is a major improvement over previous methods. To create these temporal-spatial results, we adopted or developed probability models to estimate the risk. The input data were either gathered locally or represent local conditions. Therefore, the model and the results are specific to LANL conditions while not sacrificing general flexibility for use at other regions of the country or at other time periods at LANL.

Finally, the model developed as part of this project is not complete. As discussed previously, additional terms and other sources of ignition should be incorporated into this modeling system. As a result, there appears to be a strong influence by the density of lightning flashes in this

version of the model. There may be several additional causes for this emphasis on lightning density, which can be rectified through additional work. First, many of the steps and processes that we adapted were not rigorously tested to determine their consistency with underlying assumptions. Second, some of the conclusions and methods drawn from the published literature for use in this project did not appear to be substantiated or did not fit the conditions of the Los Alamos region. Third, due to time and funding constraints, several steps in the sequence of events that lead to lightning-caused fires were not incorporated into these methods or were incorporated without amplification. Fourth, other non-lightning causes of wildfire, such as human activities, were not incorporated into these methods. Therefore, the results of the current project must be considered to be promising and informative, but preliminary.

Acknowledgments

Funding for this project was provided by the Supplemental Site-wide Environmental Impact Statement project. The land cover map used in this project was developed with the support of the Cerro Grande Rehabilitation Project and the Biological Resources Management Project. Field data used to classify the land cover map and characterize the fuels and fire hazards in the Los Alamos region were obtained through the support of the U.S. Forest Service Rocky Mountain Experiment Station and the Biological Resources Management Project. Special gratitude is extended to Terry Bott and Stephen Eisenhawer, who provided the lightning data used in this project and who provided much of the initial consultation and encouragement to the authors. Hector Hinojosa and Teresa Hiteman provided editorial and technical services. Marjorie Wright created Figures 1 and 2. Thoughtful review comments were submitted by Gene Darling, John Isaacson, David Janecky, Sam Loftin, Jack Nyhan, Susan Radzinski, and Doug Tucker.

Literature Cited

Anderson, K. 2002. A model to predict lightning-caused fire occurrences. *International Journal of Wildland Fire,* 11:163–172.

Baars, J., D. Holt, and G. Stone. 1998. Meteorological monitoring at Los Alamos. LA-UR-98-2148, Los Alamos National Laboratory, Los Alamos, New Mexico.

Balice, R.G. 1996. Biological assessment for the Dome Fire Emergency Actions. LA-UR-96-3615, Los Alamos National Laboratory, Los Alamos, New Mexico.

Balice, R.G. 1998. A preliminary survey of terrestrial plant communities in the Sierra de los Valles. LA-13523-MS, Los Alamos National Laboratory, Los Alamos, New Mexico.

Balice, R.G., S.G. Ferran, and T.S. Foxx. 1997. Preliminary vegetation and land cover classification for the Los Alamos Region. LA-UR-97-4627, Los Alamos National Laboratory, Los Alamos, New Mexico.

Balice, R.G., B.P. Oswald, and C. Martin. 1999. Fuels inventories in the Los Alamos National Laboratory Region; 1997. LA-13572-MS, Los Alamos National Laboratory, Los Alamos, New Mexico.

Balice, R.G., J.D. Miller, B.P. Oswald, C. Edminster, and S.R. Yool. 2000. Forest surveys and wildfire assessment in the Los Alamos Region; 1998–1999. LA-13714-MS, Los Alamos National Laboratory, Los Alamos, New Mexico.

Bott, T.F., and S.W. Eisenhawer. 2004. A probabilistic analysis of the risk posed by lightning during Dual-axis Radiographic Hydrodynamics Test facility high-explosives operations. LA-UR-03-8636, Los Alamos National Laboratory, Los Alamos, New Mexico.

Brook, M., N. Kitagawa, and E.J. Workman. 1962. Quantitative study of strokes and continuing currents in lightning discharges to ground. *Journal of Geophysical Research* 67:649–659.

Cummins, K.L., M.J. Murphy, E.A. Bardo, W.L. Hiscox, R.B. Pyle, and A.E. Pifer. 1998. A combined TOA/MDF technology upgrade of the U.S. National Lightning Detection Network. *Journal of Geophysical Research* 103:9035–9044.

ESRI. 2004. ArcGIS, version 9. Environmental Systems Research Institute (ESRI), Redlands, California.

Fosberg, M.A. 1972. Theory of precipitation effects on dead cylindrical fuels. *Forest Science* 18:98–108.

Fuquay, D.M. 1982. Positive cloud-to-ground lightning in summer thunderstorms. *Journal of Geophysical Research* 87:7131–7140.

Fuquay, D.M., R.G. Baughman, A.R. Taylor, and R.G. Hawe. 1967. Characteristics of seven lightning discharges that caused forest fires. *Journal of Geophysical Research* 72:6371–6373.

Fuquay, D.M., A.R. Taylor, R.G. Hawe, and C.W. Schmidt, Jr. 1972. Lightning discharges that caused forest fires. *Journal of Geophysical Research* 77:2156–2158.

Fuquay, D.M., R.G. Baughman, and D.J. Latham. 1979. A model for predicting lightning fire ignition in wildland fuels. USDA Forest Service, Research Paper INT-217, Intermountain Forest and Range Experiment Station, Ogden, Utah.

Hailwood, A.J., and S. Horrobin. 1946. Absorption of water by polymers: Analysis in terms of a simple model. *Transactions of the Faraday Society* 42B:84–92, 94–102.

Kehoe, K.E., and E.P. Krider. 2004. NLDN performance in Arizona. 18th International Lightning Detection Conference (June 7–9), Helsinki, Finland.

Kitagawa, N., M. Brook, and E.J. Workman. 1962. Continuing currents in cloud-to-ground lightning discharges. *Journal of Geophysical Research* 67:637–647.

Koch, S.W., T.K. Budge, and R.G. Balice. 1997. Development of a land cover map for Los Alamos National Lab and vicinity. LA-UR-97-4628, Los Alamos National Laboratory, Los Alamos, New Mexico.

Larjavaara, M., J. Pennanen, and T.J. Tuomi. 2005. Lightning that ignites forest fires in Finland. *Agricultural and Forest Meteorology* (in press).

Latham, D.J., and J.A. Schlieter. 1989. Ignition probabilities of wildland fuels based on simulated lightning discharges. USDA Forest Service Research Paper INT-411, Ogden, Utah.

Lewis, W.W., and C.M. Foust. 1945. Lightning investigation on transmission lines, part 7. *Transactions AIEE* 64:107–115.

McKown, B., S.W. Koch, R.G. Balice, and P. Neville. 2003. Land cover classification map for the Eastern Jemez Region. LA-14029, Los Alamos National Laboratory, Los Alamos, New Mexico.

Meteorology and Air Quality Group. 2001. The LANL weather machine: raw data request form. Web page (http://weather.lanl.gov/cgi-bin/datarequest) maintained by the Meteorology and Air Quality Group, Los Alamos National Laboratory, Los Alamos, New Mexico.

Northwestern University. 2005. The Collaboratory Project (http://collaboratory.nunet.net/), Northwestern University, Evanston, Illinois.

Orville, R.E., R.W. Henderson, and L.F. Bosart. 1983. An East Coast lightning detection network. *Bulletin of the American Meteorological Society* 64:1029–1037.

Orville, R.E., R.A. Wiesman, R.B. Pyle, R.W. Henderson, and R.E. Orville, Jr. 1987. Cloud-to-ground lightning flash characteristics from June 1984 through May 1985. *Journal of Geophysical Research* 92:5640–5644.

Rakov, V.A., and M.A. Uman. 1990. Long continuing current in negative lightning ground flashes. *Journal of Geophysical Research* 95:5455–5470.

Rakov, V.A., and M.A. Uman. 2003. *Lightning Physics and Effects*. Cambridge University Press, Cambridge, Massachusetts.

Rishel, J., S. Johnson, and D. Holt. 2003. Meteorological monitoring at Los Alamos. Progress Report, LA-UR-03-8097, Los Alamos National Laboratory, Los Alamos, New Mexico.

Shindo, T., and M.A. Uman. 1989. Continuing current in negative cloud-to-ground lightning. *Journal of Geophysical Research* 94:5189–5198.

Simpson, W.T. 1998. Equilibrium moisture content of wood in outdoor locations in the United States and worldwide. USDA Forest Service Research Note FPL-RN-0268, Madison, Wisconsin.

Site-wide Issues Program Office. 2000. A special edition of the SWEIS Yearbook: Wildfire 2000. LA-UR-00-3471, Los Alamos National Laboratory, Los Alamos, New Mexico.

Stull, R.B. 2000. *Meteorology for Scientists and Engineers*. Brooks/Cole Publishing Company, Monterey, California.

Touchan, R., C.D. Allen, and T.W. Swetnam. 1996. Fire history and climate patterns in ponderosa pine and mixed-conifer forests of the Jemez Mountains, northern New Mexico. Pages 33–46 in *Fire Effects in Southwestern Forests, Proceedings of Second La Mesa Fire Symposium* (Technical editor, C.D. Allen). General Technical Report RM-GTR-286, USDA Forest Service, Rocky Mountain Research Station, Fort Collins, Colorado.

Uman, M.A. 1987. *The Lightning Discharge*. Academic Press, Orlando, Florida.

Williams, D.P., and M. Brook. 1963. Magnetic measurements of thunderstorm currents, 1. Continuing currents in lightning. *Journal of Geophysical Research* 68:3243–3247.

U.S. Department of Energy. 1999. Site-wide environmental impact statement for continued operation of the Los Alamos National Laboratory. DOE/EIS-0238; Appendix G: Accident Analysis, U.S. Department of Energy, Albuquerque Operations Office, Albuquerque, New Mexico.

U.S. Department of Energy. 2000. Special environmental analysis for the Department of Energy, National Nuclear Security Administration: Actions taken in response to the Cerro Grande Fire at Los Alamos National Laboratory, Los Alamos, New Mexico. DOE/SEA-03, U.S. Department of Energy, Los Alamos Area Office, Los Alamos, New Mexico.

Los Alamos, New Mexico 87545